Chapter 4
Radiocarbon in the Atmosphere

J.C. Turnbull, H. Graven and N.Y. Krakauer

4.1 Introduction

Carbon dioxide (CO_2) is one of the most abundant and important atmospheric trace gases. It is found naturally in the atmosphere with a preindustrial mole fraction ("concentration") of about 280 parts per million (ppm). It is stable in the atmosphere, but exchanges readily with the surface reservoirs: the oceans (Chap. 5) and terrestrial biosphere or land (Chap. 6). Both land and oceans naturally exchange large amounts of C with the atmosphere. On long timescales, CO_2 is also removed from the atmosphere by rock weathering, but this very slow process will not be discussed further here.

The land absorbs CO_2 by photosynthetic uptake in plants and re-emits CO_2 back into the atmosphere by respiration from plants, animals, and soils (Fig. 4.1). This process produces large daily and seasonal cycles in the atmospheric CO_2 mole fraction, but on an annual to decadal timescale, the natural land exchange is nearly balanced. The gross one-way fluxes into and out of the land are about 120 petagrams of C per year (Pg C year^{-1}) (Ciais et al. 2013), but the natural net annual land flux historically was approximately zero.

J.C. Turnbull (✉)
National Isotope Centre, GNS Science, Lower Hutt, New Zealand

J.C. Turnbull
Cooperative Institute for Research in Environmental Sciences, University of Colorado, Boulder, CO, USA

H. Graven
Department of Physics and Grantham Institute for Climate Change, Imperial College London, London, UK

N.Y. Krakauer
Department of Civil Engineering, The City College of New York, New York, NY, USA

E.A.G. Schuur et al. (eds.), *Radiocarbon and Climate Change*,
DOI 10.1007/978-3-319-25643-6_4

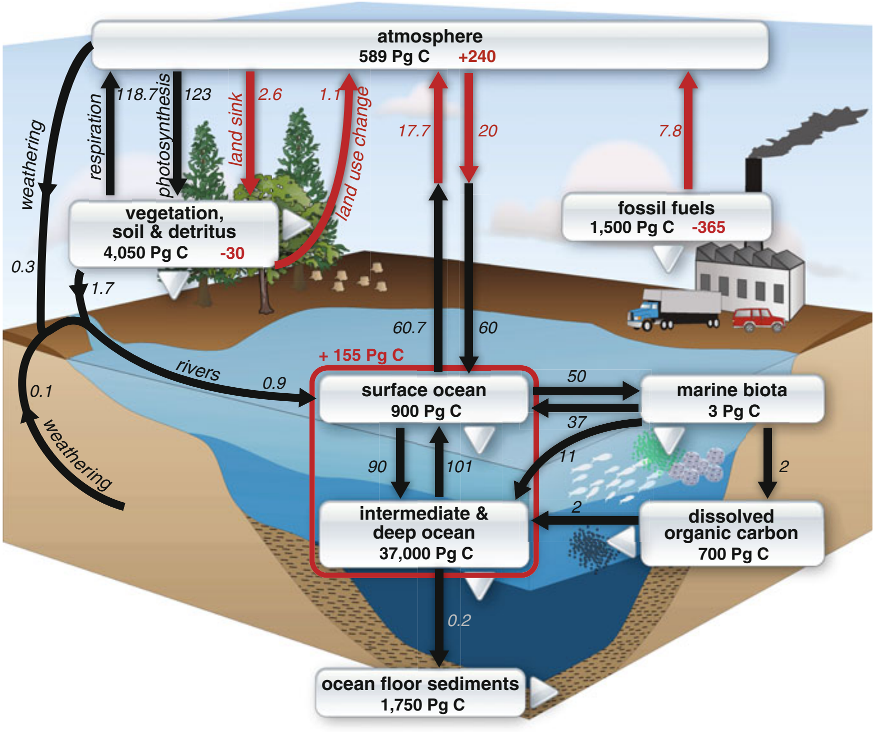

Fig. 4.1 Global C cycle showing natural C fluxes (*black*) and anthropogenic perturbations to the C cycle (*red*). Units are Pg C for pools (*boxes*) and Pg C year^{-1} for fluxes (*arrows*). Numbers shown here represent the midpoints of ranges published in Fig. 6.1 of Ciais (2013) with the exception of the soil organic matter pool that harmonizes new numbers for permafrost with global soil organic carbon inventories (Schuur et al. 2015)

Ocean C uptake and release is via gas exchange with surface waters. When upwelling water is low in dissolved CO_2, atmospheric CO_2 is absorbed and the ocean acts as a C sink. Conversely, when upwelling water is CO_2-rich, CO_2 is released and the ocean acts as a C source to the atmosphere. Many factors influence the rate of exchange, and the gross one-way fluxes into and out of the ocean are about 80 Pg C year^{-1} (Fig. 4.1), but on annual to decadal timescales, the net ocean flux was, like the land flux, roughly neutral.

Over the past 150 years, the atmosphere has been perturbed by the introduction of additional CO_2 from anthropogenic activities, primarily the combustion of fossil fuels and land-use change. The rate at which fossil fuel and land-use change C has been added to the atmosphere is small compared to the large natural fluxes, but it represents an additional one-way flux into the atmosphere that is not in balance. This results in an accelerating buildup of CO_2 in the atmosphere to the current mole fraction of over 400 ppm (in 2015). However, this increase in atmospheric CO_2 represents only about half of the ~500 Pg C emitted by humans since 1850

(Houghton 2008; Boden et al. 2012), and therefore, the other half must have moved into the ocean and land C reservoirs. Understanding exactly how much CO_2 is emitted from anthropogenic sources such as fossil fuels and land-use change, and the details of where, when, and how CO_2 is absorbed into the ocean and land is vital to predicting future atmospheric CO_2 levels and hence future climate.

Measurements of CO_2 in the atmosphere can potentially be used, in conjunction with atmospheric transport models, to infer the locations and magnitudes of the sources and sinks (release and uptake) of CO_2. Yet measurements of CO_2 mole fraction in themselves are not always sufficient to pinpoint the locations and magnitude of different sources and sinks with useful precision. Difficulties in doing so arise from the sparseness of the atmospheric measurement network, uncertainties and biases in the atmospheric transport models, and the inability to distinguish between different sources, particularly when they are located within the same region. A particular challenge is that the large gross fluxes of C into and out of the biosphere are usually the dominant source of CO_2 variability at any given time, even though on the annual timescale, the net biospheric flux is roughly in balance resulting in little or no net change in atmospheric CO_2. Radiocarbon (^{14}C) can provide a window into the atmospheric CO_2 budget, as different sources of CO_2 vary in ^{14}C content. This difference in source isotopic values allows partitioning of atmospheric observations into their component sources using standard partitioning models (Chap. 3).

In this chapter, we examine the controls on the ^{14}C content of CO_2 ($^{14}CO_2$) in the atmosphere over time in relation to CO_2 itself, and the specific C cycle questions that can therefore be addressed with atmospheric ^{14}C measurements. We discuss not only atmospheric observations, but also how these observations are interpreted using models of atmospheric transport, which describe the physical mixing of the atmosphere (similarly, models of the ocean and biosphere C reservoirs are used to describe ^{14}C movement through them). This discussion spans the simplest conceptual model of addition of a gas into a single well-mixed (homogeneous) box of air, to multibox (heterogeneous) models where the atmosphere is partitioned into a few latitudinal divisions, to full-fledged three-dimensional global or regional atmospheric transport models.

We start by examining the terms of the CO_2 and $^{14}CO_2$ budgets (Sect. 4.2). Then, we divide the atmospheric ^{14}C history into five different time periods, defined by times when different factors dominated atmospheric $^{14}CO_2$. First, we consider the preindustrial (before 1850) near steady state of $^{14}CO_2$, investigating its sources and sinks and how they differ from those of CO_2 itself (Sect. 4.3). Next, we examine the period from 1890 to 1945, when fossil fuel CO_2 emissions started to impact atmospheric $^{14}CO_2$ (the Suess effect, Sect. 4.4). The bomb period from 1945 to 1985 follows (Sect. 4.5), when the production and redistribution of ^{14}C from aboveground nuclear weapons testing produced a major perturbation in atmospheric $^{14}CO_2$ that propagated throughout the C cycle. The post-bomb period from 1985 until present is characterized by the strong dominance of fossil fuel emissions on $^{14}CO_2$ (Sect. 4.6). We also discuss how other sources are impacted, and how this can be used to examine C cycle processes. In Sect. 4.7, we suggest how atmospheric $^{14}CO_2$ might continue to evolve in the future. In Sect. 4.8, we delve into using $^{14}CO_2$ as a tracer for recently added fossil fuel CO_2, currently the most widely used application of atmospheric $^{14}CO_2$ measurements. This extended discussion of $^{14}CO_2$ is followed by related approaches using ^{14}C of other atmospheric species, including CH_4, carbon monoxide, and aerosols (Sect. 4.9). These have been less extensively studied than CO_2, but have potential for bringing new understanding to a number of atmospheric processes. Atmospheric ^{14}C is already used in a diverse suite of applications, yet there remain outstanding questions and future directions to be explored, which we address in Sect. 4.10.

4.2 Carbon Dioxide and Radiocarbon in the Atmosphere: Overview

4.2.1 The Global Carbon Dioxide and Radiocarbon Budgets

The atmospheric CO_2 budget can be described by:

$$\frac{\mathrm{d}C_\mathrm{a}}{\mathrm{d}t} = F_\mathrm{p} + F_\mathrm{r} + F_\mathrm{ao} + F_\mathrm{oa} + F_\mathrm{ff} \tag{4.1}$$

where C_a is the atmospheric CO_2 burden. F_p and F_r are the CO_2 fluxes into (photosynthesis) and out of (respiration, biomass burning, etc.) the terrestrial biosphere. From an atmospheric perspective, C uptake or release by vegetation due to land-use change is indistinguishable from natural terrestrial C exchange and is therefore implicitly included in these terms. F_ao and F_oa are the fluxes from the atmosphere into the ocean and from the ocean into the atmosphere, respectively. F_ff is the flux into the atmosphere from fossil fuel emissions. In this notation, fluxes into the atmosphere (F_r, F_oa, F_ff) are positive, and fluxes out of the atmosphere (F_p, F_ao) are negative.

The change in ^{14}C can be described in a similar way as follows:

$$\frac{\mathrm{d}C_\mathrm{a}\Delta_\mathrm{a}}{\mathrm{d}t} = F_\mathrm{p}\Delta_\mathrm{p} + F_\mathrm{r}\Delta_\mathrm{r} + F_\mathrm{ao}\Delta_\mathrm{ao} + F_\mathrm{oa}\Delta_\mathrm{oa} + F_\mathrm{ff}\Delta_\mathrm{ff} + F_\mathrm{c}\Delta_\mathrm{c} + F_\mathrm{n}\Delta_\mathrm{n} + F_\mathrm{d}\Delta_\mathrm{d} \tag{4.2}$$

where Δ is the ^{14}C value of the denoted pool or flux (Tans et al. 1979). The ^{14}C budget has three extra terms. All of these terms are pure ^{14}C fluxes, with, by definition, ^{14}C of 8.5×10^{14} ‰, so although the fluxes are very small, the impact on $^{14}CO_2$ can be large. F_c is the flux due to natural cosmogenic production of ^{14}C in the upper atmosphere. F_n is the flux due to (1) atmospheric nuclear weapons testing (bomb ^{14}C) and (2) the nuclear industry—primarily nuclear reactors, but also including spent nuclear fuel reprocessing and other ^{14}C production, such as ^{14}C created for isotopic labeling experiments and subsequently released to the atmosphere. This term comprises ^{14}C atoms created by humans. F_d is the negative flux due to radioactive decay, which is too small to influence decadal to century-scale changes in atmosphere ^{14}C and is ignored hereafter. This equation describes the entire atmosphere as a single pool, but since the stratosphere, as the primary site of cosmogenic production, is enriched in ^{14}C relative to the troposphere, it can be treated as a separate pool (Levin et al. 2010). Combining Eqs. 4.1 and 4.2, we obtain

$$C_{\mathrm{a}}\frac{\mathrm{d}\Delta_{\mathrm{a}}}{\mathrm{d}t} = F_{\mathrm{r}}(\Delta_{\mathrm{r}} - \Delta_{\mathrm{a}}) + F_{\mathrm{oa}}(\Delta_{\mathrm{oa}} - \Delta_{\mathrm{a}}) + F_{\mathrm{ff}}(\Delta_{\mathrm{ff}} - \Delta_{\mathrm{a}}) + F_{\mathrm{c}}(\Delta_{\mathrm{c}} - \Delta_{\mathrm{a}}) + F_{\mathrm{n}}(\Delta_{\mathrm{n}} - \Delta_{\mathrm{a}}) + F_{\mathrm{p}}(\Delta_{\mathrm{p}} - \Delta_{\mathrm{a}}) + F_{\mathrm{ao}}(\Delta_{\mathrm{ao}} - \Delta_{\mathrm{a}}) \tag{4.3}$$

Each term on the right-hand side of Eq. 4.3 is an *isoflux*, the product of the one-way gross CO_2 flux and the isotopic difference between the source (or sink) and the atmosphere. This difference is known as the isotopic disequilibrium. A small CO_2 flux can have a large isoflux if the isotopic disequilibrium between the atmosphere and the reservoir is large, and conversely, a large CO_2 flux can have a small or zero isoflux if there is little or no isotopic disequilibrium between the atmosphere and the reservoir. Isofluxes may be positive or negative, depending on the sign of the isotopic disequilibrium, and the isoflux may be of a different sign than the CO_2 flux. When C is dissolved into the surface ocean or taken up by plants (fixed by photosynthesis), the only change in isotopic composition is due to mass-dependent fractionation during uptake, which is corrected for in the ^{14}C nomenclature (Chap. 3). Therefore, p and ao are by definition equal to a, so the isotopic disequilibrium in uptake is zero. As a result, the last two terms in Eq. 4.3 that represent the isofluxes into the biosphere and oceans are equal to zero, and

$$C_{\mathrm{a}}\frac{\mathrm{d}\Delta_{\mathrm{a}}}{\mathrm{d}t} = F_{\mathrm{r}}(\Delta_{\mathrm{r}} - \Delta_{\mathrm{a}}) + F_{\mathrm{oa}}(\Delta_{\mathrm{oa}} - \Delta_{\mathrm{a}}) + F_{\mathrm{ff}}(\Delta_{\mathrm{ff}} - \Delta_{\mathrm{a}}) + F_{\mathrm{c}}(\Delta_{\mathrm{c}} - \Delta_{\mathrm{a}}) + F_{\mathrm{n}}(\Delta_{\mathrm{n}} - \Delta_{\mathrm{a}}) \tag{4.4}$$

The remaining terms in Eq. 4.4 are all fluxes of CO_2 into the atmosphere. So measurements of $^{14}CO_2$ detect the one-way gross fluxes into the atmosphere, rather than the net fluxes that are detected by CO_2 concentration measurements.

Four factors drive the isotopic disequilibrium in ^{14}C between the sources and the atmosphere: (1) natural production of ^{14}C by interaction of nitrogen with cosmic rays in the upper atmosphere; (2) anthropogenic production of ^{14}C from nuclear weapons testing and the nuclear industry; (3) fossil fuel emissions; and (4) the *reservoir age*, which determines the ^{14}C content in each C reservoir or source. Radiocarbon decays in reservoirs that are out of contact with the atmosphere, resulting in lower ^{14}C, which can also be presented in terms of the ^{14}C age or reservoir age in units of years by relating ^{14}C to the decay rate of ^{14}C. The reservoir age can be determined from the ^{14}C content of the atmosphere at the time the C was taken up into the reservoir, together with the residence time of C in that reservoir. It can also be determined empirically from measurements of the reservoir's ^{14}C value.

4.2.2 *Atmospheric Transport Modeling of Radiocarbon*

Interpretation of atmospheric observations of $^{14}CO_2$ and CO_2 requires an understanding of the movement and mixing of air, as well as the sources and sinks of CO_2. Carbon cycle and atmospheric transport models are used to build up detailed descriptions of these interactions, and these descriptions can be tested and adjusted by comparison with observations. The global budgets of both CO_2 and $^{14}CO_2$, described in Eqs. 4.1 and 4.2, can be simulated by models with varying degrees of resolution and complexity. Models of the terrestrial biosphere and ocean provide information on the flux of C and the isotopic disequilibrium from each reservoir, taking changes in atmospheric ^{14}C into account. One example of this type of modeling exercise is the global budgeting of CO_2 and $^{14}CO_2$ isofluxes for different time periods shown in Tables 4.1, 4.2, and 4.3. Simulated isofluxes include uncertainties that are the subject of ongoing research. These uncertainties relate to the transport rates and pathways of C on land and in the ocean and the difficulty in representing ecosystem and oceanic dynamics in models (Naegler and Levin 2009b; Levin et al. 2010; Graven et al. 2012b, c). Uncertainty in the cosmogenic ^{14}C production rate is also significant, with various estimates differing by ~25 % (Lal 1988; Masarik and Beer 1999). The source of CO_2 from fossil fuel combustion is

Table 4.1 Idealized steady-state preindustrial ^{14}C isofluxes to the atmosphere

Reservoir	Estimated flux F into the atmosphere (Pg C year^{-1})	$\Delta^{14}C$ difference between reservoir and atmosphere (‰)	Isoflux (Pg C ‰ year^{-1})	Impact on $\Delta^{14}CO_2$ (‰ year^{-1})
Oceans	85 ± 21[a]	−65[b]	−5500 ± 1400	−9 ± 2
Terrestrial biosphere	52 ± 11[c]	−4.5[c]	−235 ± 55	−0.4 ± 0.1
Cosmogenic production	$6.5 \pm 0.8 \times 10^{-12}$ [d]	8.5×10^{14}	5500 ± 700	9 ± 1
Annual mean change			0	0

The isoflux is the product of the C flux and the isotopic difference between the reservoir and the preindustrial atmosphere ($a = 0$ ‰). The impact of each isoflux on atmospheric $^{14}CO_2$ is calculated assuming a preindustrial CO_2 mixing ratio of 280 ppm. Cosmogenic production generates pure ^{14}C, which equates to a $\Delta^{14}C$ value of 8.5×10^{14} ‰

[a] Heimann and Maier-Reimer (1996)

[b] Key et al. (2004)

[c] Naegler and Levin (2009b)

[d] Lal (1988), Masarik and Beer (1999)

Table 4.2 Estimated ^{14}C isofluxes to the troposphere in 1963 near the start of the bomb period

Reservoir	Estimated flux F into the atmosphere (Pg C year^{-1})	Δ^{14}C difference between reservoir and atmosphere (‰)	Isoflux (Pg C ‰ year^{-1})	Impact on $\Delta^{14}CO_2$ (‰ year^{-1})
Fossil fuels	2.8 ± 0.3[a]	−1570[f]	−4400 ± 400	−7 ± 1
Ocean	85 ± 21[b]	−635[g]	−54,000 ± 13,000	−80 ± 20
Terrestrial biosphere	52 ± 11[c]	−575[c]	−30,000 ± 6000	−44 ± 9
Nuclear weapons testing	2.6×10^{-10} [d]	8.5×10^{14}	220,000	320
Cosmogenic production	$6.5 \pm 0.8 \times 10^{-12}$ [e]	8.5×10^{14}	5500 ± 700	8 ± 1
Annual mean change			+140,000	+200

The isoflux is the product of the C flux and the isotopic difference between the reservoir and the atmosphere (tropospheric $\Delta^{14}CO_2$ = 570 ‰ for 1963; Levin et al. 2010). The impact of each isoflux on atmospheric $^{14}CO_2$ is calculated assuming an atmospheric CO_2 mixing ratio of 319 ppm for 1963 (Keeling and Whorf 2005). Note that this budget omits ^{14}C accumulation in the stratosphere

[a] Marland et al. (2006), including 10 % uncertainty in emissions

[b] Heimann and Maier-Reimer (1996)

[c] Naegler and Levin (2009b), assuming negligible change in ^{14}C from preindustrial state

[d] Levin et al. (2010)

[e] Lal (1988), Masarik and Beer (1999)

[f] Zero ^{14}C content, or −1000 ‰ in fossil C

[g] Key et al. (2004), assuming negligible change in ^{14}C from preindustrial state

estimated using economic data on fuel use and carries an uncertainty of 5–10 % for global emissions (Marland 2010).

Thus far, we have used Eq. 4.4 to describe the global ^{14}C budget, yet we often want to understand the C budget in smaller regions. The biosphere, fossil fuel, and nuclear isofluxes are all predominantly over the Northern Hemisphere land. In contrast, the ocean exchange is concentrated in the Southern Ocean, due to upwelling of old water and fast wind-driven air–sea exchange there. These geographic differences result in a north–south interhemispheric gradient in $^{14}CO_2$. The cosmogenic production source is concentrated in the upper atmosphere at higher latitudes because of the structure of the Earth's magnetic field, but is roughly symmetric between the two hemispheres (e.g., Lal 1988). There is also considerable heterogeneity in the isofluxes at regional scales and through time. The mixing timescale of the troposphere between hemispheres is about one year; it involves barriers associated with the intertropical convergence zone near the equator, as well as divergent subtropical and convergent subpolar regions (Jacob 1999). Mixing occurs more rapidly in the west–east direction over the mid-latitudes of each hemisphere due to predominantly zonal winds, with a timescale of a few weeks.

Table 4.3 Estimated ^{14}C isofluxes to the atmosphere in 1995 (post-bomb period)

Reservoir	Estimated flux F into the atmosphere (Pg C year^{-1})	Δ^{14}C difference between reservoir and atmosphere (‰)	Isoflux (Pg C ‰ year^{-1})	Impact on $\Delta^{14}CO_2$ (‰ year^{-1})
Fossil fuels	6.4 ± 0.6[a]	-1115[f]	-7100 ± 700	-9 ± 1
Ocean	85 ± 21[b]	-60[g]	-5100 ± 1200	-7 ± 2
Terrestrial biosphere	52 ± 11[c]	25 ± 25[c]	1300 ± 1500	2 ± 2
Nuclear weapons testing	8×10^{-13} [d]	8.5×10^{14}	700	1
Cosmogenic production	$6.5 \pm 0.8 \times 10^{-12}$ [e]	8.5×10^{14}	5500 ± 700	7 ± 1
Annual mean change			-4700	-6

The isoflux is the product of the C flux and the isotopic difference between the reservoir and the atmosphere (using a atmospheric $\Delta^{14}CO_2$ = 115 ‰ for 1995; Levin et al. 2010). The impact of each isoflux on atmospheric $^{14}CO_2$ is calculated assuming an atmospheric CO_2 mixing ratio of 361 ppm for 1995 (Keeling and Whorf 2005). Note that if mixing is assumed to occur only in the troposphere, then these values increase by about 25 %

[a] Marland et al. (2006), including 10 % uncertainty in emissions

[b] Heimann and Maier-Reimer (1996)

[c] Naegler and Levin (2009b)

[d] UNSCEAR (2000)

[e] Lal (1988), Masarik and Beer (1999)

[f] Zero ^{14}C content, or −1000 ‰ in fossil C

[g] Key et al. (2004)

Mixing with the stratosphere is slower, with a timescale of several years (Jacob 1999). This variability in the isofluxes and in atmospheric mixing results in spatial and temporal variability in ^{14}C and in CO_2 mole fraction in the atmosphere.

Atmospheric observations are made at specific locations, and the atmospheric variability needs to be understood to interpret these measurements at global, regional, and local scales. Atmospheric transport models are commonly used to address this. These models use a combination of theoretical formulations and observations of meteorological parameters to describe atmospheric transport. The isofluxes are then input to the model and convolved with the transport to obtain simulated atmospheric ^{14}C and CO_2 mole fractions.

The simplest atmospheric transport models are box models that divide the atmosphere into a few compartments or *boxes*, such as the GRACE model (Levin et al. 2010). Typically, the global atmosphere is divided into 2–8 zonal bands and/or separated vertically into troposphere and stratosphere boxes. A separate stratosphere is particularly important for describing vertical gradients of ^{14}C, since this is the initial location of both cosmogenic ^{14}C production and bomb-produced ^{14}C. These simple box models typically work on time steps of one year. At each time step, an estimated isoflux from each source (biosphere, ocean, fossil fuels, nuclear industry, and cosmogenic production) is entered into each box. The isoflux estimates are best guesses that are usually determined offline from other models or information. The isofluxes are mixed between the atmospheric boxes using simple parameterizations of the mixing rates between the various boxes. These box models can approximate the overall latitudinal patterns observed in both CO_2 concentration and in ^{14}C isotope ratios, and can be used to test isoflux estimates. Simple models are computationally cheap, so they are often used to examine variability over long time periods of hundreds to thousands of years. However, their simplicity means that they cannot adequately describe more detailed regional and temporal variability.

More complex global atmospheric transport models divide the world into many more boxes. Typically, the Earth's surface is gridded into boxes of up to a few degrees (100–500 km) on a side, and between 15 and 100 vertical levels. As computing time and storage become cheaper, these models are moving to higher resolution (more gridboxes). These models usually ingest meteorological observations to *force* the transport, but can also be driven by their own physics-based simulation of atmospheric transport, or some combination of the two. The largest difficulty comes in dealing with phenomena that occur at a smaller scale than the gridboxes and must be *parameterized*, convective mixing being one example. These models are immensely helpful in understanding observed distributions. They are widely used in *inversions*, a method of adjusting the a priori flux estimates to optimize the agreement between observations and model simulations (Gurney et al. 2002). Typically, a set of a priori flux estimates are obtained from bottom-up inventory information and/or process models such as terrestrial and ocean C cycle models and gridded to the same spatial and temporal scale as the atmospheric transport model. These fluxes are ingested into the model to provide simulated ^{14}C and CO_2 mole fractions. The simulated and observed values are compared, and adjustments (typically using least squares minimization) are made to the fluxes to improve the agreement between the two, obtaining improved flux estimates, known as a posteriori fluxes. Thus far, $^{14}CO_2$ inversions have been done in only a simplified way, whereby model simulations are performed with several different sets of a priori fluxes to test which fluxes agree best with the observations (e.g., Turnbull et al. 2011).

However, more work is needed to improve the accuracy of the atmospheric transport models. Most atmospheric transport models do not accurately predict the vertical transport of tracers such as CO_2, leading to too much or not enough accumulation in the surface boundary layer (Stephens et al. 2007). As yet, only a handful of simulations with three-dimensional atmospheric transport models have been performed with a complete depiction of the ^{14}C isofluxes (Randerson et al. 2002; Turnbull et al. 2009b; Miller et al. 2012). These studies have shown that over the continents in the post-bomb period (since 1985), the ^{14}C variability is usually dominated by the fossil fuel isoflux (Sect. 4.6). Thus, the models can be used to simulate continental $^{14}CO_2$ gradients resulting from fossil fuels and compare them to observed $^{14}CO_2$ gradients (Sect. 4.8).

Regional models are similar to global atmospheric transport models, but allow increased spatial and temporal resolution by modeling only a small portion of the atmosphere. They typically cover regions with spatial extent of a few hundreds to thousands of kilometers and often only examine the lower regions of the atmosphere. The higher resolution is beneficial for regional studies, but these models must address "boundary conditions"—the mixing ratios and isotopic values of air entering the edges of the model domain (Hsueh et al. 2007; Palstra et al. 2008; Riley et al. 2008). At much smaller scales of tens to hundreds of meters, plume models provide an alternative modeling method. These describe the dispersion of a plume of gas within the atmosphere and can be useful for describing atmospheric enrichment near a source, such as that caused by ^{14}C emissions from nuclear power plants (Levin et al. 2003) or emissions from point sources (Turnbull et al. 2014). At distances of more than a few kilometers from a source, their assumptions usually break down.

4.3 Preindustrial Distribution of Radiocarbon

In the preindustrial atmosphere before 1850, the fossil fuel and nuclear isofluxes were zero, so only cosmogenic production, radioactive decay, and land and ocean exchanges influenced atmospheric $^{14}CO_2$. Cosmogenic production was the only positive isoflux, increasing ^{14}C in the atmosphere by about 9 ‰ year^{-1} (Table 4.1). Both the terrestrial biosphere and oceans had negative isofluxes, since C resides in each of these reservoirs for some time and becomes depleted in ^{14}C by radioactive decay before returning to the atmosphere. The biospheric residence time is typically years or decades (Chap. 6), whereas the ocean reservoir age is typically hundreds or thousands of years (Chap. 5). Therefore, in the preindustrial atmosphere, the ocean isoflux by far dominated over the land isoflux (Table 4.1) in its influence on $^{14}CO_2$ variability.

4.3.1 *Mean Isotope Ratio*

The ^{14}C content of CO_2 in the past atmosphere can be measured from C samples with known ages, such as tree rings. These can be analyzed for ^{14}C content today, which can be converted to past ^{14}C (Chap. 3) by counting the exact age of each tree ring and correcting for radioactive decay that occurred since the time of growth. Considerable effort has been made to construct tree-ring chronologies for paleoclimate applications (Chap. 7), and the tree-ring record presently extends ~14,000 years before 1950 ("before present" or BP) (Friedrich et al. 2004; Hua et al. 2009). Reconstruction of atmospheric $^{14}CO_2$ content goes beyond this, back to the detection limit of ^{14}C measurements at ~50,000 years BP, based on ^{14}C in cross-dated coral carbonate and foraminifera (Reimer 2013). Neither corals nor foraminifera reflect the atmospheric $^{14}CO_2$ content as precisely as tree rings because their ^{14}C is different from atmospheric $^{14}CO_2$ due to the ocean reservoir age (Reimer 2013). Uncertainty in the reservoir age and its variability through time make the reconstruction of atmospheric $^{14}CO_2$ content in the distant past potentially less accurate than the measurements from tree rings.

In a steady-state Earth system, $^{14}CO_2$ will be constant, with cosmogenic ^{14}C being produced in the atmosphere, then mixing throughout the C reservoirs, where it radioactively decays. Table 4.1 shows the globally integrated $^{14}CO_2$ isofluxes for an idealized preindustrial steady state, where cosmogenic ^{14}C production in the atmosphere is balanced almost entirely by C exchange with the oceans, which have lower ^{14}C due to radioactive decay within the oceans themselves. Biospheric exchange makes a smaller contribution to the preindustrial $^{14}CO_2$ balance since the land biosphere has a much shorter mean C residence time and smaller C pool than the oceans.

Yet the Earth System is dynamic, and records show that $^{14}CO_2$ has varied through time, due to variability in both cosmogenic production and in the global C cycle. The various records show that $^{14}CO_2$ increases when the cosmogenic ^{14}C production rate increases (F_c in Eq. 4.4), while it decreases when the atmospheric CO_2 concentration increases and dilutes the ^{14}C content (in Eq. 4.4, increasing C_a results in decreased a). During the last ice age, when the atmospheric CO_2 concentration was up to 35 % lower than during interglacial periods, $\Delta^{14}CO_2$ was as high as +600 ‰ (Reimer 2013) (Fig. 4.2). Over the last 10,000 years, $\Delta^{14}CO_2$ has stayed within a 100 ‰ range, mostly decreasing gradually, and showed quasi-cyclic variations on decade to century timescales associated with solar activity, which drives changes in cosmogenic ^{14}C production (Stuiver and Braziunas 1993). Millennial and longer scale fluctuations in $^{14}CO_2$ are largely correlated with the Earth's magnetic field strength, which also affects the ^{14}C production rate (Mazaud et al. 1991). By assuming that the C cycle (i.e., plant photosynthesis and respiration and ocean CO_2 exchange) was constant over the Holocene, the $^{14}CO_2$ record can be inverted to yield a time series of smoothed fluctuations in cosmogenic ^{14}C production (Usoskin and Kromer 2005). However, part of

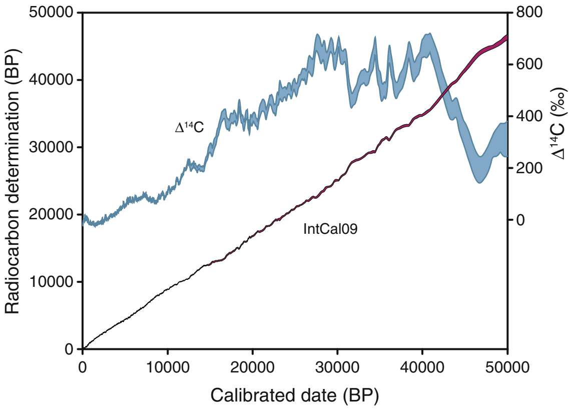

Fig. 4.2 The IntCal09 calibration curve and age-corrected $\Delta^{14}C$ (‰) with one standard deviation envelopes. Figure modified from Reimer et al. (2009)

the $^{14}CO_2$ variability is likely due to changes in the C cycle, driven for example by ocean upwelling variability (Muscheler et al. 2004; Kohler et al. 2006). A simple box model of the C cycle performed better in reproducing the higher $^{14}CO_2$ in the last ice age if exchange between surface and deep ocean water is decreased by 50 % and the shell carbonate sedimentation rate is decreased by 10 % compared with Holocene values (Hughen et al. 2004). In the preindustrial atmosphere, the biosphere likely did not have a large impact on $^{14}CO_2$ gradients, even if the biospheric CO_2 flux varied, since the biospheric turnover time is on the order of decades, and the ^{14}C of respired CO_2 was therefore only slightly lower than atmospheric $^{14}CO_2$ (Braziunas et al. 1995). This topic is also covered in more detail in Chap. 7.

4.3.2 Spatial Gradients

The reconstructions of $^{14}CO_2$ show hemispheric and regional variability (Hua and Barbetti 2004; Hua et al. 2013) due to the spatial distribution of the isofluxes, with the ocean isoflux concentrated in the Southern Hemisphere, the biospheric isoflux mostly in the Northern Hemisphere, and the cosmogenic isoflux at high altitudes near the poles (Sect. 4.2.2). The mixing timescale of the troposphere is about one year between hemispheres, but only a few weeks in the west–east direction at the mid-latitudes of each hemisphere. Due to the faster mixing time in the longitudinal direction, along with the primarily latitudinal pattern of spatial variability in the fluxes, latitudinal variability in preindustrial $^{14}CO_2$ was characteristically much greater than longitudinal variability. Models have shown that preindustrial longitudinal gradients are likely below the detection limit of present-day measurement techniques because of the fast mixing in the west–east direction (Fig. 4.3, Braziunas

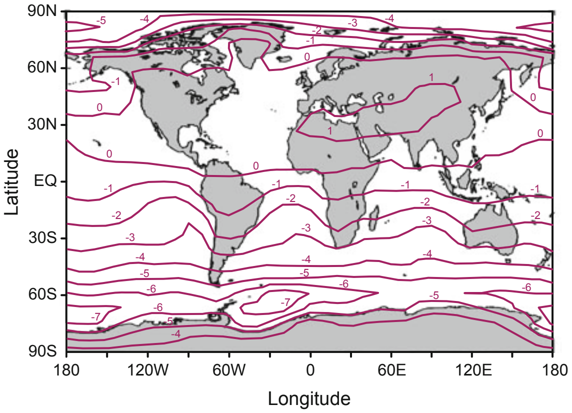

Fig. 4.3 Geographic distribution of simulated preindustrial atmospheric $\Delta^{14}C$. Contours are in units of permil and represent deviations from a fixed value of 0 ‰ for the Olympic Peninsula, Washington, USA. Figure modified from Braziunas et al. (1995)

et al. 1995). Most studies have therefore focused on the larger preindustrial latitudinal gradients, particularly the interhemispheric difference.

The first accurate measurements of the interhemispheric gradient in preindustrial $^{14}CO_2$ showed that Southern Hemisphere tree-ring samples from the 1830s had $\Delta^{14}CO_2$ 4.5 ± 1 ‰ lower than Northern Hemisphere samples (Lerman et al. 1970). Subsequent studies found similar north–south offsets from mid-latitude sites in the late eighteenth to the late nineteenth centuries (Vogel et al. 1993; McCormac et al. 1998; Stuiver and Braziunas 1998). This preindustrial interhemispheric difference is primarily due to the predominance of the ocean isoflux in the Southern Hemisphere. In addition to the large ocean surface area there, upwelling of old water and fast wind-driven air–sea exchange increase the Southern Ocean isoflux. Two studies (Hogg et al. 2002; McCormac et al. 2002) analyzed decadal-average tree-ring samples from Great Britain and New Zealand going back to 950 AD, with replicate measurements conducted in the Belfast and Waikato laboratories to control for interlaboratory calibration differences. They found an average difference of 5.0 ± 1.6 ‰ over 950–1850, but with detectable centennial-scale variability of up to ±4 ‰ (Fig. 4.4). The variability has been attributed to changing wind patterns over the Southern Ocean during the Medieval warm period and the Little Ice Age (Rodgers et al. 2011). Such analyses are at the edge of the accuracy of current measurement technology and require stringent calibration and quality control procedures. Recent work, making use of newly developed, longer New Zealand tree chronologies, finds interhemispheric offsets for the first millennium AD that are similar in magnitude and variability to those of the preindustrial second millennium (Hogg et al. 2009b). With a lower degree of precision, *wiggle matching* (matching the timescales by lining up the patterns of variability in ^{14}C) with floating Southern Hemisphere tree-ring chronologies extends this conclusion through previous millennia in the Holocene (Hogg et al. 2009a).

Less attention has been paid to reconstructing preindustrial $^{14}CO_2$ in regions outside the mid-latitudes. The complexity of atmospheric transport in the tropics is illustrated by work with Thai trees (19°N) from the seventeenth and eighteenth

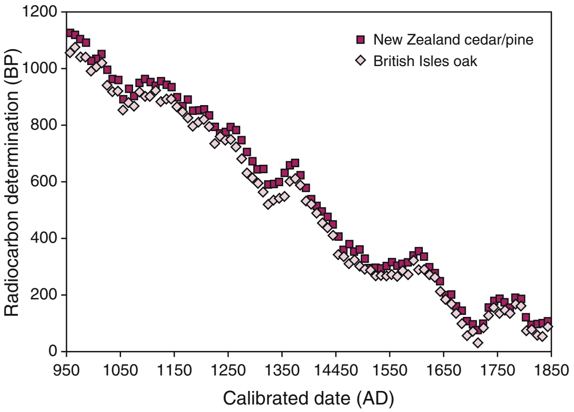

Fig. 4.4 Radiocarbon ages of independently dated Southern and Northern Hemisphere wood. Figure modified from Hogg et al. (2002)

centuries, which showed that $^{14}CO_2$ levels were intermediate between those of northern and southern mid-latitudes despite their location in the Northern Hemisphere (Hua et al. 2004). This is attributed to northward entrainment of Southern Hemisphere air, with lower $^{14}CO_2$, during the Asian summer monsoon.

4.4 The “Suess” Period: 1890–1945

The first observation of anthropogenic influence on atmospheric $^{14}CO_2$ was made by Suess (1955), showing decreasing $^{14}CO_2$ in the early part of the 1900s in tree-ring records from North America. The decline in atmospheric $^{14}CO_2$ content since the industrial revolution demonstrated the addition of ^{14}C-free fossil fuel CO_2 to the atmosphere (Fig. 4.5a). Suess’ tree-ring measurements showed a decrease of 25 ‰ in atmospheric $\Delta^{14}CO_2$ between 1890 and 1950 (Suess 1955). This decrease, now called the *Suess effect*, is not determined solely by the rate of fossil fuel

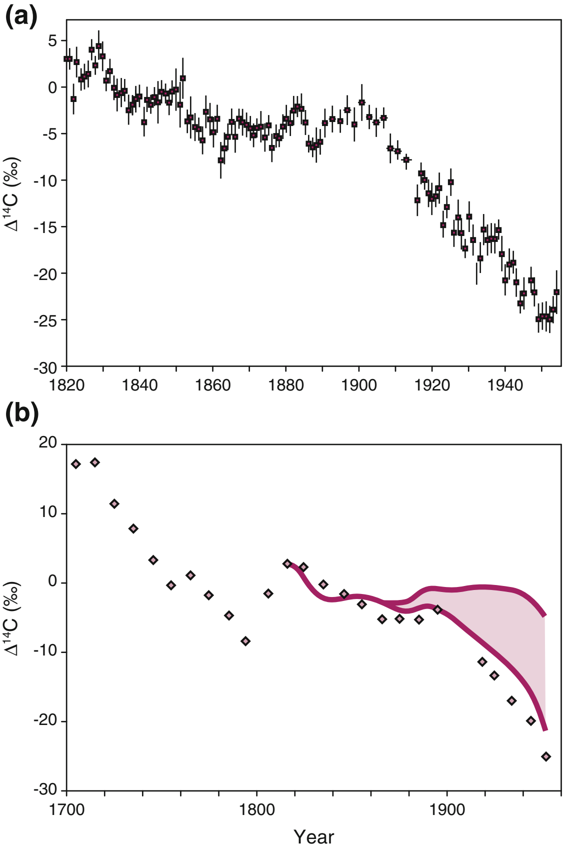

Fig. 4.5 (**a**) Observations of $\Delta^{14}C$ in tree rings from the Northwestern US. (**b**) Carbon cycle model of $\Delta^{14}CO_2$ calculated for the natural atmospheric $^{14}CO_2$ level (top line) and taking into account the release of fossil CO_2 (bottom line). Symbols are observed $^{14}CO_2$ values. Figures modified from Stuiver and Quay (1981)

emissions, however. Gross fluxes of C between the atmosphere and the oceans and terrestrial biosphere moderate the dilution of atmospheric $^{14}CO_2$ by effectively increasing the reservoir of C into which the ^{14}C-free fossil fuel CO_2 is mixed. Via gross exchanges, some fossil-derived C enters the oceanic and terrestrial reservoirs and is replaced in the atmosphere by C with the ^{14}C of the oceanic and terrestrial reservoirs.

Representation of the Suess effect in models of the global C cycle is sensitive to the exchange rates associated with air–land and air–ocean fluxes (Revelle and Suess 1957; Oeschger et al. 1975; Stuiver and Quay 1981). In one of the first applications of a C cycle model, the observed Suess effect was used in a very simple box model that included one atmospheric box and one oceanic box to estimate the global air–sea exchange rate (Revelle and Suess 1957). Since then, the Suess effect has been simulated in more advanced C cycle models, including one that also considered how the observed Suess effect might have been influenced by variations in cosmogenic ^{14}C production (Fig. 4.5b, Stuiver and Quay 1981). Utilizing a model with various possible relationships between ^{14}C production and the observed number of sunspots between 1735 and 1952, this study demonstrated that the observed decrease in $^{14}CO_2$ could not have been caused by natural fluctuations in cosmogenic production.

Further compilation of tree-ring records from different locations provided an early indication that the magnitude of the Suess effect varied regionally. The decrease in $^{14}CO_2$ until the 1930s was 5–10 ‰ greater in European trees than in North American trees (Tans et al. 1979; De Jong and Mook 1982). These observations demonstrated that the Suess effect was enhanced in regions with strong local combustion sources, a finding that would later be exploited to estimate regional fossil fuel CO_2 emission rates (Sect. 4.8.1).

4.5 The “Bomb” Period: 1945–1985

The first direct measurements of $^{14}CO_2$ in the atmosphere were made in 1954 in New Zealand (Rafter and Fergusson 1957; Currie et al. 2011). Globally distributed networks of ground-based atmospheric sampling stations followed shortly after (Nydal 1963; Manning et al. 1990; Levin et al. 1992). These networks were initially deployed to observe the radioactive fallout caused by intensive nuclear weapons testing in the 1950s and 1960s. Production of ^{14}C by nuclear weapons testing nearly doubled the tropospheric burden of $^{14}CO_2$ in the Northern Hemisphere (Fig. 4.6). In the Northern Hemisphere, $^{14}CO_2$ peaked in 1963 with the maximum of large aboveground thermonuclear (hydrogen fusion) bomb tests immediately before the atmospheric nuclear test ban treaty came into effect. In the Southern Hemisphere, $^{14}CO_2$ peaked a few years later. $^{14}CO_2$ then began to decrease rapidly as the negative isoflux from the ocean and terrestrial biosphere became larger than the positive isoflux from the stratosphere (Figs. 4.5a and 4.6). The observed trend in $^{14}CO_2$ resembled an exponential curve, initially falling rapidly (by more than 40 ‰ year^{-1})

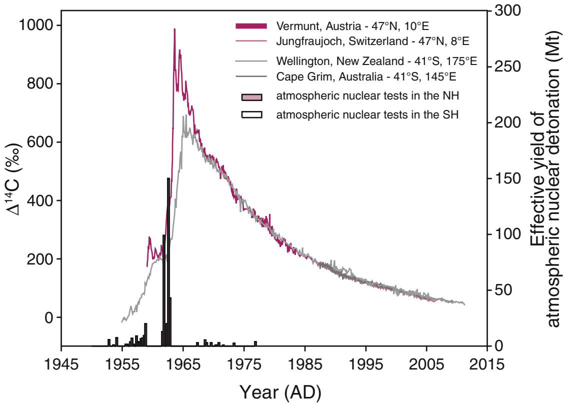

Fig. 4.6 Observations of $\Delta^{14}CO_2$ and the magnitude of nuclear explosions occurring in the Northern Hemisphere (*black lines* and *bars*) and Southern Hemisphere (*gray lines* and *white bars*). Figure modified from Hua and Barbetti (2007), with observations from Levin and Kromer (2004), Currie et al. (2011) and Levin et al. (2010)

then slowing with time (Fig. 4.6). Estimated isofluxes for the start of the bomb period are shown in Table 4.2.

Due to the long half-life of ^{14}C, excess ^{14}C produced by weapons testing will remain for many thousands of years. As discussed for fossil fuel CO_2 and the Suess effect, the natural C cycle exchange acts to redistribute this bomb ^{14}C throughout the atmosphere, biosphere, and oceans. The rate of redistribution of bomb ^{14}C provides a method for tracing natural C exchanges that has been used in many aspects of C cycle studies. In this section, we will describe the input of ^{14}C to the atmosphere from weapons testing and the initial transfers of bomb ^{14}C between C reservoirs, focusing on the influence of these processes on atmospheric $^{14}CO_2$ and how these observations have been used to study atmospheric C exchange.

4.5.1 Global Bomb Radiocarbon Budget

Most of the nuclear weapons tests occurred in the Northern Hemisphere (UNSCEAR 2000) (Fig. 4.6), and the explosive force injected ^{14}C into the stratosphere roughly 10–17 km above sea level. The large initial concentration of bomb ^{14}C in the northern stratosphere was observed using high-altitude aircraft, revealing $\Delta^{14}CO_2$ values as large as 5000–20,000 ‰ in the stratosphere (Telegadas 1971; Hesshaimer and Levin 2000). Bomb ^{14}C gradually entered the troposphere via stratosphere–troposphere exchange processes in the mid- to high latitudes. Investigation of the time-evolving budget of bomb ^{14}C in C cycle studies and assessment of the human exposure to radioactive fallout requires estimates of the total amount of ^{14}C produced by weapons testing (Fig. 4.7). These estimates use emission factors that assume ^{14}C produced in each test was roughly proportional to the explosive force of the bomb (e.g., UNSCEAR 2000). There are significant uncertainties in these estimates of bomb ^{14}C production since the production of neutrons may vary with different types of fuel or bomb designs and not all neutrons react to produce ^{14}C. Several studies have augmented estimates from scaling factors with observations of bomb-derived ^{14}C and C cycle models (e.g., Hesshaimer et al. 1994; Naegler and Levin 2006). The current best estimate of total bomb ^{14}C is 598–632 × 10^{26} atoms (Naegler and Levin 2006). Though a few tests were performed after the nuclear test ban in 1963, almost all bomb ^{14}C was produced by thermonuclear bomb tests between 1961 and 1963 (Fig. 4.6). For comparison, it would take 250 years to produce this amount of ^{14}C cosmogenically (Masarik and Beer 1999). Besides the strong pulse of ^{14}C from bomb testing, a small amount of anthropogenic ^{14}C production continues to occur through nuclear industrial and research applications (UNSCEAR 2000). Annual anthropogenic ^{14}C production comprised approximately 10 % of natural cosmogenic production in recent decades (Graven and Gruber 2011).

Since all of the bomb ^{14}C produced must be allocated into atmospheric, oceanic, or terrestrial reservoirs, accounting for bomb ^{14}C in a realistic C cycle model constrained with observations of bomb ^{14}C in the troposphere, stratosphere, and ocean can help to refine the estimates of the total bomb ^{14}C produced. By creating ^{14}C budgets that incorporate information from C cycle models, bomb ^{14}C observations, and bomb detonation histories, researchers have also argued for a lower estimate of the air–ocean gas exchange rate (Hesshaimer et al. 1994) and provided an estimate of the total biospheric inventory of bomb ^{14}C (Naegler and Levin 2009a) (Fig. 4.7). The total biospheric inventory of bomb ^{14}C can provide a useful measure of the average residence time and ^{14}C disequilibrium of terrestrial C, which

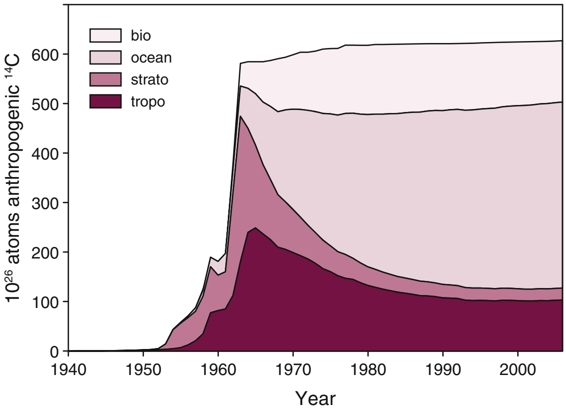

Fig. 4.7 The time-evolving global inventory of anthropogenic ^{14}C, derived primarily from bomb testing but also from ongoing ^{14}C production by the nuclear power industry, in tropospheric, stratospheric, terrestrial, and oceanic reservoirs. Figure modified from Naegler and Levin (2009b)

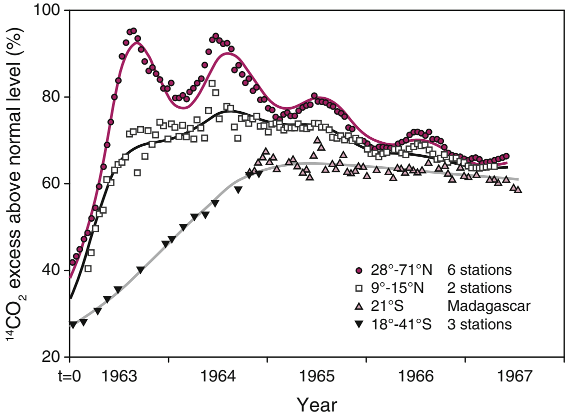

Fig. 4.8 Observations of $\Delta^{14}CO_2$ during the early bomb period, from stations grouped by latitude. Figure modified from Nydal and Lovseth (1983)

is difficult to observe directly because of the heterogeneity in biomass and ecosystem types (Chap. 6).

4.5.2 Atmospheric Radiocarbon Seasonality During the Bomb Period

The seasonal cycles of $^{14}CO_2$ had amplitudes of more than 100 ‰ at Northern Hemisphere ground-level stations in the mid-1960s (Fig. 4.8). These observations clearly demonstrated the strong seasonality in the descent of stratospheric, bomb ^{14}C-enriched air across the tropopause (Nydal and Lovseth 1965), showing that the strength of stratosphere-to-troposphere exchange has a maximum in late spring in each hemisphere. The seasonal maximum in $^{14}CO_2$ at ground level occurred in summer, delayed by a few months from the strongest stratosphere–troposphere exchange due to the time required for air to descend from the upper troposphere to ground level. The magnitude of the seasonal amplitude was influenced by heterotrophic respiration, which still had prebomb ^{14}C values, resulting in strongly negative isofluxes to the atmosphere (Randerson et al. 2002). As heterotrophic respiration is strongest in summer, this isoflux offset the stratospheric input and slightly reduced seasonal amplitudes from what they otherwise would have been.

4.5.3 Spatial Gradients

By tracing the movement of bomb ^{14}C through the atmosphere, early $^{14}CO_2$ observations helped to establish the rates and seasonality of stratosphere-to-troposphere exchange and of latitudinal and cross-equatorial mixing of the troposphere. Strong latitudinal gradients in the troposphere were created by the concentrated bomb ^{14}C input to the northern latitudes where nuclear weapons were tested and subsequent transport of that bomb ^{14}C through the troposphere. Observed $\Delta^{14}CO_2$ was 100–500 ‰ higher at northern stations than at southern stations between 1961 and 1965 (Figs. 4.6 and 4.7). Strong latitudinal gradients were also present within the Northern Hemisphere, where observed $\Delta^{14}CO_2$ values were 20–200 ‰ higher at mid- to high latitudes than low latitudes (Fig. 4.8).

Observed $\Delta^{14}CO_2$ values during the bomb period were used to estimate that the timescale of interhemispheric mixing across the equator is approximately one year (Lal and Rama 1966; Nydal 1968). This mixing timescale is an important determinant of latitudinal gradients of CO_2 and several industrial gases, since their emissions and surface exchanges occur primarily in the Northern Hemisphere. Therefore, accurate representation of interhemispheric mixing is essential for model-based estimates of regional fluxes of CO_2 and other gases (Denning et al. 1999). The early $^{14}CO_2$ observations have also been used to constrain cross-equatorial and cross-tropopause exchange in atmospheric box models (Lal and Rama 1966; Nydal 1968; Johnston 1994; Naegler and Levin 2006) and to test three-dimensional atmospheric general circulation models (Kjellstrom et al. 2000; Land et al. 2002). In addition to providing a chemical tracer to estimate transport rates, observations of $^{14}CO_2$ and other radioactive fallout species have also helped in developing theories on internal stratospheric dynamics and stratosphere–troposphere exchange (Holton et al. 1995).

Latitudinal gradients observed in the bomb period were also influenced by the spatial distribution of terrestrial, oceanic, and fossil fuel isofluxes (globally integrated isofluxes for 1963 are summarized in Table 4.2). During the period of testing and the subsequent few years, these influences were minor in comparison with the effect of the bombs and stratospheric ^{14}C input to the Northern Hemisphere. However, after 1968, stratospheric ^{14}C input decreased substantially and latitudinal gradients became much smaller. In the late 1960s and early 1970s, stratospheric and oceanic isofluxes made roughly equal contributions to the interhemispheric $^{14}CO_2$ gradient, each increasing Northern Hemisphere $\Delta^{14}CO_2$ by 10–20 ‰, compared to the Southern Hemisphere (Randerson et al. 2002; Levin et al. 2010; Fig. 4.9c). Even though negative isofluxes were occurring over the entire ocean, the isofluxes were the largest over the Southern Ocean due to stronger air–sea ^{14}C gradients and high winds (see also Chap. 5). Stronger negative isofluxes over the Southern Ocean decreased Southern Hemisphere $^{14}CO_2$ values relative to Northern Hemisphere $^{14}CO_2$ values, reinforcing the gradient caused by stratospheric ^{14}C input in the north. Small negative isofluxes from the biosphere and fossil fuel emissions, focused over the tropics and northern continents, counteracted the stratospheric and oceanic influences on latitudinal gradients (Randerson et al. 2002; Levin et al. 2010; Fig. 4.9c).

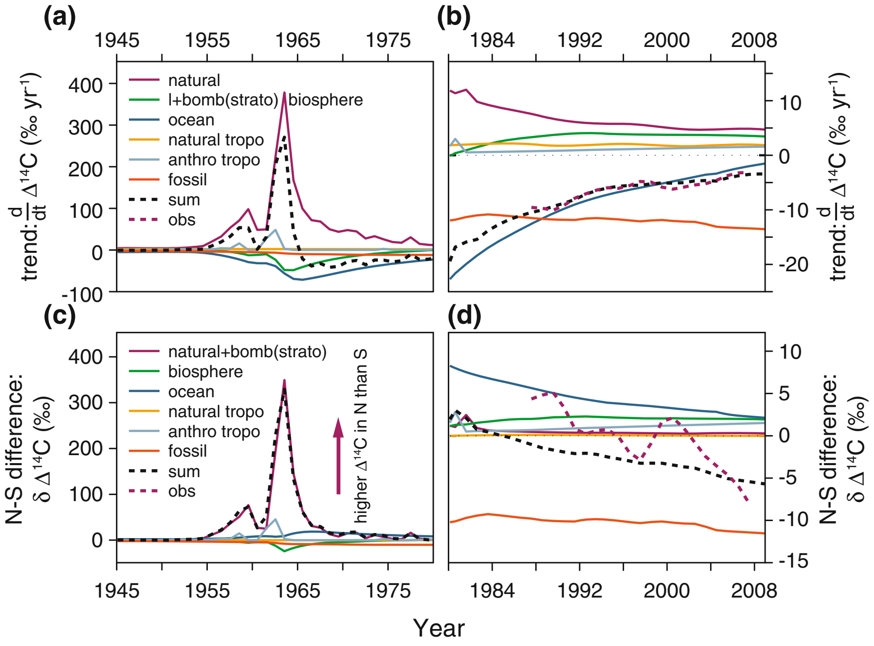

Fig. 4.9 Simulated components of the global tropospheric $^{14}CO_2$ trend (**a**, **b**) and North–South interhemispheric gradient (**c**, **d**) for 1945–1980 (**a**, **c**) and 1980–2008 (**b**, **d**). The *black dashed line* shows the sum of all simulated components, and the *purple dashed line* in the *right panels* shows the observed global trend (**b**) and the observed gradient between Jungfraujoch and Cape Grim, 1987–2007 (**d**). Figure modified from Levin et al. (2010)

4.5.4 Evolving Isofluxes During the Bomb Period

As bomb ^{14}C dispersed through the atmosphere and entered oceanic and terrestrial reservoirs, changes to $^{14}CO_2$ and the subsequent changes in the ^{14}C of oceanic and terrestrial C caused ^{14}C isofluxes to evolve. For example, in 1963, respiration of short-term C pools in the terrestrial biosphere, such as leaves and twigs, added CO_2 that was fixed before the peak in $^{14}CO_2$. Therefore, the ^{14}C of leaves and twigs was much lower than $^{14}CO_2$ and the respiration of leaves and twigs caused a large negative isoflux (Fig. 4.9a; Table 4.2). By 1975, a large fraction of the C in leaves and twigs had been fixed after the peak in $^{14}CO_2$ and the respiration of leaves and twigs contributed much less to the decreasing trend in $^{14}CO_2$. Since the amount and average residence time of C in the terrestrial biosphere is smaller than in the ocean, the negative isoflux from the terrestrial biosphere was smaller and decreased more rapidly than the oceanic isoflux (Randerson et al. 2002; Naegler and Levin 2009a; Levin et al. 2010). Negative isofluxes from fossil fuel emissions were much smaller than the negative isoflux from the ocean and terrestrial biosphere before 1970, but after 1970 fossil fuel emissions became a principal influence on the decreasing trend in $^{14}CO_2$.

4.6 The Post-bomb Period: 1985–Present

We consider the post-bomb period as the period commencing in the mid-1980s, after a few decades had passed since the peak $^{14}CO_2$ level in the troposphere and the influences on atmospheric $^{14}CO_2$ had changed significantly. The rapid uptake of bomb ^{14}C during the bomb period that decreased the tropospheric $^{14}CO_2$ content simultaneously increased ^{14}C in land biosphere and ocean reservoirs. In the post-bomb period, rapidly overturning C reservoirs came closer to equilibrium with tropospheric $^{14}CO_2$, while at the same time, uptake of bomb ^{14}C into longer term reservoirs continued and fossil fuel emissions increased. These processes changed the disequilibrium in terrestrial, oceanic, and stratospheric C reservoirs, thereby altering the influence of those exchanges on tropospheric $^{14}CO_2$ (Fig. 4.9b, d). The start of this period is somewhat arbitrary, since the processes are continuous, but we consider this period to start when the global biosphere isoflux changed sign in about the mid-1980s (Randerson et al. 2002; Naegler and Levin 2009b). This section will describe the influences on the long-term trend, interhemispheric gradient, and seasonal cycles in tropospheric $^{14}CO_2$ over the post-bomb period, including how each process changed since the bomb period.

The history of $^{14}CO_2$ through the post-bomb period has been directly measured by continued measurements from a few locations. The longest records, both of which continue today, are from New Zealand (Currie et al. 2011) and the European Alps (Levin and Kromer 2004), shown in Fig. 4.6. Observations from these and several other shorter records from around the globe are available from the Carbon Dioxide Information Analysis Center (http://cdiac.ornl.gov/). In recent years and decades, additional observations of $^{14}CO_2$ at both clean-air and polluted measurement sites have begun at laboratories in Europe (Levin et al. 2010; Van Der Laan et al. 2010), the US (Turnbull et al. 2007; Graven et al. 2012b, c) and Japan (Kitigawa et al. 2004).

4.6.1 Fossil Fuel Carbon Dioxide

CO_2 emissions from fossil fuel burning have grown substantially over the post-bomb period, increasing by ~50 % between 1985 and 2005 (Marland et al. 2006). Dilution of $^{14}CO_2$ by fossil-derived CO_2 is now the strongest contribution to the long-term trend and interhemispheric gradient of $^{14}CO_2$ in unpolluted background air (Fig. 4.9) and is one of the main influences on seasonal cycles of $^{14}CO_2$ in the Northern Hemisphere (Levin et al. 2010; Graven et al. 2012b, c). Fossil fuel CO_2 emissions decreased tropospheric $\Delta^{14}CO_2$ by about 10 ‰ year^{-1} (Table 4.3).

Despite the large growth in fossil fuel emissions, their influence on the $^{14}CO_2$ trend and interhemispheric gradient has remained rather steady over the post-bomb period (Levin et al. 2010; Graven et al. 2012b, c; Fig. 4.9b). This can be attributed to a decrease in the sensitivity of $^{14}CO_2$ to fossil fuel emissions between the 1980s and 2000s: The troposphere–fossil fuel isotopic disequilibrium grew smaller as $\Delta^{14}CO_2$ dropped from 250 to 50 ‰ and the fractional change in the CO_2 mixing ratio caused by an added increment of fossil fuel CO_2 grew smaller as tropospheric CO_2 increased from 350 ppm to the 2014 level of about 395 ppm (Levin et al. 2010; Graven et al. 2012c).

4.6.2 Nuclear Industry

The growth of nuclear power over the post-bomb period also has an impact on $^{14}CO_2$ because ^{14}C is released from nuclear power plants and fuel reprocessing sites, causing small, continual increases to the global inventory of ^{14}C (UNSCEAR 2000; Levin et al. 2010; Graven et al. 2012b). Globally, this term is small, at about 0.5–1 ‰ year^{-1} increase in $\Delta^{14}CO_2$ (Table 4.3), but it can be important at the local and regional scale (Graven and Gruber 2011).

4.6.3 Terrestrial Carbon

By the 1980s, the terrestrial biosphere had assimilated ~20 % of the total bomb ^{14}C, and mean ^{14}C of respired C was close to that of tropospheric $^{14}CO_2$ (Randerson et al. 2002; Naegler and Levin 2009b). In essence, the terrestrial biosphere had nearly reached equilibrium with tropospheric $^{14}CO_2$ after roughly 20 years. Yet, as tropospheric $^{14}CO_2$ continued to decline due to air–ocean exchange and fossil fuel emissions, complete equilibrium could not be reached. Atmospheric $^{14}CO_2$ became, on average, lower than the ^{14}C of C respired by terrestrial ecosystems. Thus, in the post-bomb period, the net effect of terrestrial respiration was to return bomb ^{14}C back to the troposphere (Fig. 4.7), and the biospheric isoflux reversed sign (Randerson et al. 2002; Naegler and Levin 2009b; Levin et al. 2010; Fig. 4.10). Regionally, terrestrial ecosystems release C of various ages during heterotrophic respiration, and ecosystems in different locations can release C with different mean ages (Chap. 6). Therefore, although the global average near-equilibrium in ^{14}C distribution was reached in the 1980s, this near-equilibrium was reached sooner in the tropics where C cycling is rapid, and later in boreal and arctic systems where C cycling is slower (Randerson et al. 2002).

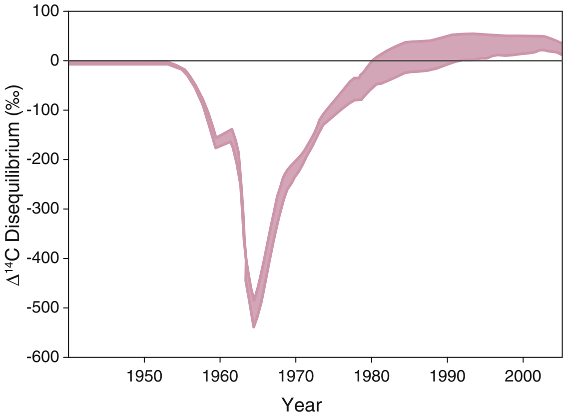

Fig. 4.10 Disequilibrium between Δ^{14}C in terrestrial respiration and tropospheric CO_2 over 1940–2005 as simulated by a two-box biosphere model. Figure modified from Naegler and Levin (2009b)

4.6.4 Oceans

Water at the ocean surface is composed of varying mixtures of young water that has recently been in contact with the air and older water that has been sequestered in the deep ocean for centuries (Chap. 5). Because of this, the ocean surface has even stronger regional variability in the mean age of C exchanged with the air than does the terrestrial biosphere. Water in subtropical gyres does not mix readily with deeper water and maintains close contact with the atmosphere, while in the Southern Ocean and North Pacific Ocean, there is a significant fraction of old water that has been upwelled from depth after being out of contact with the atmosphere for hundreds to thousands of years.

In the post-bomb period, water in the subtropical gyres contains a large amount of bomb ^{14}C that has not been dispersed by mixing with deeper water, and thus, isofluxes here resemble those from the terrestrial biosphere. They do incorporate some upwelled water that is depleted in ^{14}C; however, the source of upwelling is shallow, relatively young water that has already assimilated some bomb ^{14}C. Thus, subtropical areas of the ocean had reached near-equilibrium with tropospheric $^{14}CO_2$ by 1995, when large-scale hydrographic surveys showed that ^{14}C values in surface waters of the subtropics were nearly the same as tropospheric $^{14}CO_2$ values (Key et al. 2004; Graven et al. 2012a) (Fig. 4.10). Since 1995, ^{14}C values in these ocean regions has become even higher than tropospheric $^{14}CO_2$ values (Graven et al. 2012a). Like the terrestrial biosphere, these subtropical surface waters have started to release bomb ^{14}C back to the atmosphere where $^{14}CO_2$ content continues to decrease; thus, the isoflux has changed sign.

In contrast, in both the Southern Ocean and North Pacific Ocean, significant uptake of bomb ^{14}C is still occurring. Since surface waters in these regions mix with deep water, into which bomb ^{14}C has not yet intruded, ^{14}C there is still substantially depleted in comparison with the troposphere and has not come to this near-equilibrium state (Key et al. 2004; Graven et al. 2012a; Fig. 4.10). The

Southern Ocean is the dominant region of oceanic influence on atmospheric $^{14}CO_2$, with large regions of negative ocean–atmosphere gradients stronger than 100 ‰ as compared to gradients of 50–100 ‰ over smaller areas in the North Pacific. In the Southern Ocean, strong circumpolar winds drive strong upwelling of deep, ^{14}C-depleted water and enhance gas transfer, leading to strong negative isofluxes. These isofluxes cause $^{14}CO_2$ to be reduced in air above the Southern Ocean (Levin and Hesshaimer 2000; Randerson et al. 2002; Fig. 4.11).

Globally, the integrated flux of bomb ^{14}C into the ocean over the bomb and post-bomb periods provides a strong constraint on the average gas exchange velocity (Chap. 5; Revelle and Suess 1957; Broecker et al. 1985; Sweeney et al. 2007). Other estimates of the average gas exchange velocity must extrapolate from point measurements of ocean–atmosphere fluxes, which results in large uncertainties (Frost and Upstill-Goddard 1999). Both oceanic and atmospheric ^{14}C measurements have been crucial in estimating and refining the global mean gas exchange velocity (Hesshaimer et al. 1994; Krakauer et al. 2006; Naegler and Levin 2006), which is needed to calculate the magnitude and locations of uptake of anthropogenic CO_2 by the ocean using observations of ocean–atmosphere gradients in pCO_2 (Takahashi et al. 2009).

Over the post-bomb period, the integrated flux of bomb ^{14}C into the oceans has diminished and global ocean bomb ^{14}C inventories in the 2000s are nearly stagnant (Graven et al. 2012a), due to near balance between the high-latitude uptake and

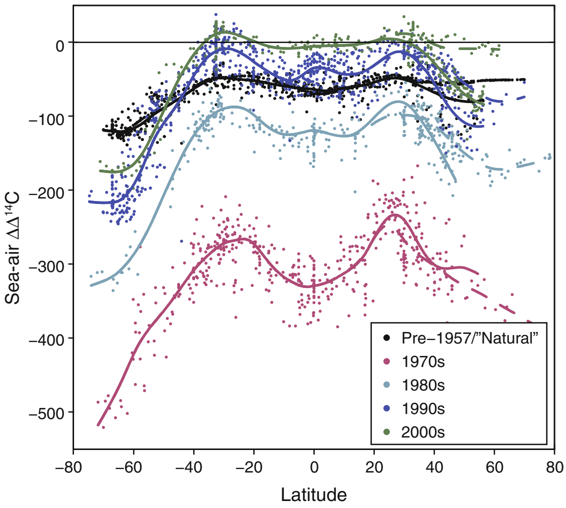

Fig. 4.11 Ocean–atmosphere gradients in Δ^{14}C versus latitude by decade in the bomb and post-bomb periods. Estimates of preindustrial surface water Δ^{14}C (Key et al. 2004) or observations made prior to 1957 are compared to the preindustrial atmospheric ^{14}C of 0 ‰ and shown in *black*. *Solid lines* show smoothed curves for data in all regions south of 30°N and in the North Pacific, north of 30°N. *Dashed lines* show smoothed curves for data in all regions south of 30°N and in the North Atlantic, north of 30°N. Figure modified from Graven et al. (2012a)

low-latitude release of bomb ^{14}C. As the low-latitude release surpasses high-latitude uptake, the oceans are now beginning an overall transfer of bomb ^{14}C back to the atmosphere.

4.6.5 Stratosphere

In the post-bomb period, the stratosphere continues to be enriched in ^{14}C relative to the troposphere, even though the bomb ^{14}C that was initially injected into the stratosphere has dispersed. Observations of $\Delta^{14}CO_2$ in stratospheric air indicate that it was 50–150 ‰ above that measured in the troposphere in the early 1990s (Turnbull et al. 2009b; Fig. 4.12). One reason for higher ^{14}C content in the stratosphere during the post-bomb period is that most cosmogenic production of ^{14}C occurs in the stratosphere (O'Brien 1979; Jöckel 1999). While the natural stratosphere–troposphere gradient was amplified by the input of bomb ^{14}C, the stratosphere–troposphere gradient has been positive throughout history due to this effect. Another reason for higher ^{14}C content in the stratosphere during the post-bomb period is the residence time of air in the stratosphere, on the order of five-to-ten years, which creates a lag in stratospheric response to the surface exchanges that are reducing tropospheric $^{14}CO_2$.

This stratosphere–troposphere $^{14}CO_2$ gradient continues to be exploited in studies of cross-tropopause transport of air and stratospheric residence times during the post-bomb period. Observed stratosphere–troposphere gradients of $^{14}CO_2$ in 1989–1990 were used to estimate an average turnover time of the stratosphere of

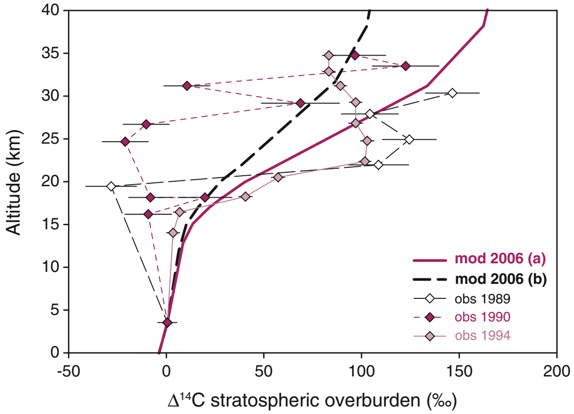

Fig. 4.12 Vertical profiles of stratospheric $\Delta^{14}CO_2$ above Japan (40°N) in 1989–94, relative to $\Delta^{14}CO_2$ in the free troposphere, from stratospheric and high tropospheric samples taken in 1989, 1990, and 1994. Two model simulations for 2006 are shown, model (**a**) uses cosmogenic production from Lal (1988), model (**b**) moves the production to lower altitudes within the stratosphere. Figure modified from Turnbull et al. (2009b)

~9 years (Nakamura et al. 1992, 1994). In addition, very strong vertical gradients observed within the stratosphere indicate vertical mixing of stratospheric air is slow. Investigation of stratosphere–tropospheric dynamics can also utilize ^{14}CO, the dominant form of newly produced ^{14}C atoms which oxidizes to $^{14}CO_2$ over a timescale of weeks to months (Jöckel and Brenninkmeijer 2002; Sect. 4.9.1).

4.6.6 Long-Term Trend

In the post-bomb period, there is a complex interplay between positive influences on tropospheric $^{14}CO_2$ from the terrestrial biosphere, low-latitude oceans, stratosphere and nuclear industry, and negative influences from the high-latitude oceans and fossil fuel combustion (Levin et al. 2010; Graven et al. 2012b, c; Fig. 4.9b; Table 4.3). The long-term trend of tropospheric $^{14}CO_2$ continues to be negative (Figs. 4.6 and 4.9b), although the rate of decline has slowed from 10 ‰ year^{-1} in the 1980s to 5 ‰ year^{-1} since 2000 (Meijer et al. 2006; Levin et al. 2010). The primary cause of this slowing is the weakening effect of ocean–atmosphere exchange, which has resulted in the emergence of fossil fuel emissions as the dominant influence on tropospheric $^{14}CO_2$. Since 2000, all influences on $^{14}CO_2$ each contribute less than ±5 ‰ year^{-1} to the trend, except for fossil fuel emissions, which contribute −10 to −15 ‰ year^{-1} (the exact magnitude varies slightly through time and depends on whether CO_2 from fossil fuel emissions is assumed to mix into the entire atmosphere or only into the troposphere) (Levin et al. 2010; Graven et al. 2012b; Fig. 4.9b).

4.6.7 Interhemispheric Gradient

The observed interhemispheric gradient of $^{14}CO_2$ was close to zero over most of the post-bomb period, reflecting a near balance between the effect of fossil fuel emissions and other processes (Randerson et al. 2002; Meijer et al. 2006; Levin et al. 2010; Fig. 4.9d). The dilution of $^{14}CO_2$ by fossil fuel emissions in the Northern Hemisphere was offset primarily by air–sea exchange that decreased $^{14}CO_2$ in the Southern Hemisphere. ^{14}C release by terrestrial ecosystems and nuclear power plants, concentrated in the Northern Hemisphere, also counteracted the effect of fossil fuel emissions. Since 2000, $^{14}CO_2$ in the Northern Hemisphere has become lower than $^{14}CO_2$ in the Southern Hemisphere (Levin et al. 2010; Graven et al. 2012c), apparently due to a reduction in the ^{14}C isoflux from the Southern Ocean. However, the total interhemispheric gradient simulated by models has not matched the observed gradient over the post-bomb period, and the changing interhemispheric gradient has not yet been fully explained (Randerson et al. 2002; Levin et al. 2010).

4.6.8 Seasonal Cycles

Seasonal cycles in $^{14}CO_2$ were much smaller during the post-bomb period than during the bomb period (Randerson et al. 2002; Levin et al. 2010; Fig. 4.13). The largest cycles now occur at northern mid- and high-latitude sites, which show amplitudes of several permil with maxima in late summer or fall (Meijer et al. 2006; Turnbull et al. 2007; Levin et al. 2010; Graven et al. 2012c). Seasonality in $^{14}CO_2$ primarily results from seasonal variations in atmospheric transport that regulates the stratospheric and fossil fuel isofluxes, rather than seasonality in the isofluxes themselves. As during the bomb period, the seasonal input of stratospheric air increases $^{14}CO_2$ in summer and fall at mid- to high latitudes, although the effect is much smaller in the post-bomb period (Randerson et al. 2002; Levin et al. 2010). Although fossil fuel CO_2 emissions themselves have only a small seasonal cycle, more vigorous atmospheric mixing during summer and fall allows fossil fuel CO_2 emissions to be transported away from the surface and mixed into a larger volume of air, increasing local tropospheric $^{14}CO_2$ relative to the winter months (Randerson et al. 2002; Turnbull et al. 2009a; Levin et al. 2010; Graven et al. 2012c). Smaller effects result from terrestrial and oceanic exchanges. Stronger summertime respiration slightly enriches $^{14}CO_2$ in summer months in the Northern Hemisphere, and stronger ocean–atmosphere exchange slightly depletes $^{14}CO_2$ in winter months over the Southern Ocean (Randerson et al. 2002; Turnbull et al. 2009a; Levin et al. 2010).

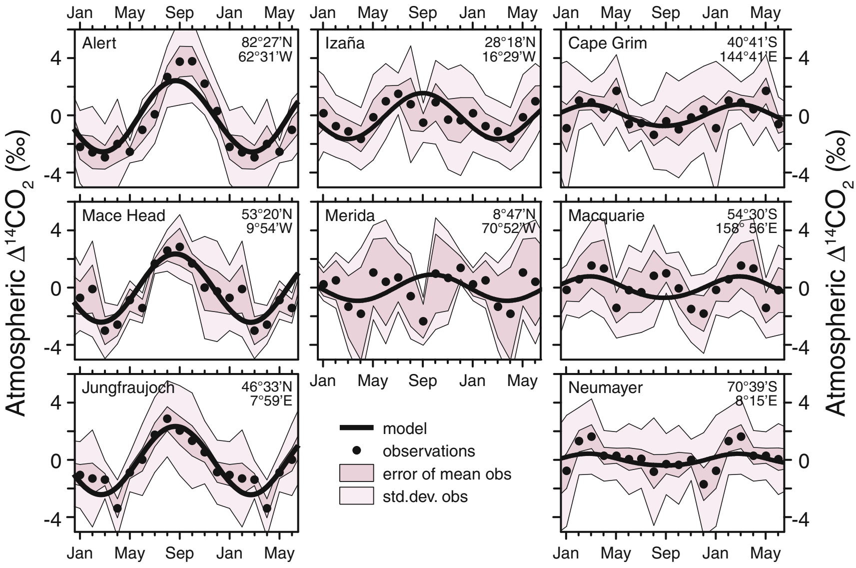

Fig. 4.13 Observed and simulated average seasonal cycles of $\Delta^{14}CO_2$ for sites in the Heidelberg University observation network over 1995–2005. Figure modified from Levin et al. (2010)

4.7 The Future Trajectory of Atmospheric Radiocarbon

Tropospheric $\Delta^{14}CO_2$ is now (in 2014) about 30 ‰, that is, 3 % above the preindustrial level. If fossil fuel emissions continue to increase in a "business-as-usual" scenario (Ciais et al. 2013), atmospheric $\Delta^{14}CO_2$ values will likely drop below the preindustrial level (0 ‰) within the next decade. The continued decrease in $^{14}CO_2$ will cause the C reservoirs in the land and surface ocean that are presently enriched in ^{14}C to sustain their positive isofluxes to the atmosphere, while negative isofluxes from ^{14}C-depleted reservoirs such as the Southern Ocean will become weaker as their disequilibrium with $^{14}CO_2$ is reduced. Atmospheric $\Delta^{14}CO_2$ values may reach −150 ‰ by the year 2100 (Caldeira et al. 1998; Fig. 4.14). At this point, even the deep waters upwelling in the Southern Ocean will return CO_2 enriched in ^{14}C to the atmosphere and become a positive isoflux. Observation of such changes in the coming decades will continue to illuminate the C cycle exchange processes that determine how ^{14}C is redistributed in response to anthropogenic perturbations.

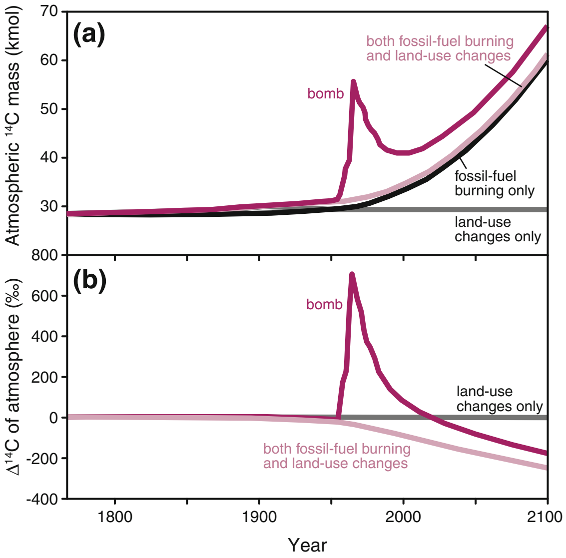

Fig. 4.14 Model simulations of the atmospheric ^{14}C inventory and $^{14}CO_2$ over 1765–2100 for scenarios in which perturbations from land-use change only, land-use change and fossil fuel burning or land-use change, fossil fuel burning and bomb testing were included. Figure modified from Caldeira et al. (1998)

4.8 Atmospheric Monitoring of Fossil Fuel Carbon Dioxide Emissions

4.8.1 Determination of Fossil Fuel Mole Fraction from Radiocarbon Observations

In recent years, atmospheric $^{14}CO_2$ measurements have been recognized as the most unambiguous tracer method to quantify fossil fuel CO_2 (CO_{2ff}) emissions. Due to the influence of the fossil fuel isoflux on atmospheric $^{14}CO_2$ gradients, $^{14}CO_2$ can provide an objective method of evaluating the CO_{2ff} emissions reported by governments and industry. Equally importantly, the separation of fossil fuel and biological CO_2 sources by $^{14}CO_2$ allows examination of biological CO_2 exchange processes.

In order to calculate the amount of fossil fuel CO_2 present in an atmospheric sample in which $^{14}CO_2$ has been measured, the mass balances for C and ^{14}C from Eqs. 4.1 and 4.2 are integrated to:

$$CO_{2obs} = CO_{2bg} + CO_{2ff} + CO_{2other} \tag{4.5}$$

and

$$\Delta_{obs}CO_{2obs} = \Delta_{bg}CO_{2bg} + \Delta_{ff}CO_{2ff} + \Delta_{other}CO_{2other}, \tag{4.6}$$

then manipulated to solve for CO_{2ff}:

$$CO_{2ff} = \frac{CO_{2obs}(\Delta_{obs} - \Delta_{bg})}{\Delta_{ff} - \Delta_{bg}} - \frac{CO_{2other}(\Delta_{other} - \Delta_{bg})}{\Delta_{ff} - \Delta_{bg}}. \tag{4.7}$$

To emphasize the influence of fossil fuel combustion, the other terms have been condensed into a single CO_{2other} term, which is essentially a correction for non-fossil influences on $^{14}CO_2$. This represents CO_2 added or removed by non-fossil sources or sinks (respiration and biomass burning, nuclear industry, and to a lesser extent the oceans and cosmogenic production) and Δ_{other} represents the weighted mean ^{14}C of the other CO_2 sources. The integration adds two other terms, CO_{2bg} and Δ_{bg}, which represent the background air CO_2 mixing ratio and its $\Delta^{14}CO_2$ value, respectively. In this approach, the “background” is chosen to represent the initial composition of a parcel of air, which then moves across a region of interest, modifying its CO_2 mole fraction and $^{14}CO_2$ by the addition of CO_{2ff} and CO_{2other}. An upwind clean-air reference site can be assumed to represent the background; this is especially useful when examining large-scale gradients in $^{14}CO_2$ across continents.

In Eq. 4.7, ^{14}C of photosynthetic uptake (gross primary productivity) is implicitly assumed to be equal to Δ_{bg}. This is strictly true in the limit that the time (and space) between background and observation goes to zero. Some authors (e.g., Kuc et al. 2007; Riley et al. 2008) have instead assumed that ^{14}C of photosynthesis is equal to Δ_{obs}, and in this case, Eq. 4.7 can be rewritten as follows:

$$CO_{2ff} = \frac{CO_{2bg}(\Delta_{obs} - \Delta_{bg})}{\Delta_{ff} - \Delta_{obs}} - \frac{CO_{2other}(\Delta_{other} - \Delta_{obs})}{\Delta_{ff} - \Delta_{obs}} \tag{4.8}$$

When integrated $^{14}CO_2$ sampling (e.g., absorption onto NaOH over a period of days or weeks) is used, this formulation may be advantageous, as CO_{2obs} is not required, but the mean CO_{2bg} must be estimated. In the case of flask sampling, CO_{2obs} will usually be directly measured from the same flask, so Eq. 4.7 is more convenient. If CO_{2other} is zero, then Eqs. 4.7 and 4.8 are exactly equivalent, but slight differences in the calculated CO_{2ff} of up to 0.1 ppm can occur when both photosynthetic uptake of CO_2 and the $\Delta_{obs} - \Delta_{bg}$ differences are large (Turnbull et al. 2009a). These differences are small relative to the current CO_{2ff} detection capability.

In the current atmosphere, with about 395 ppm CO_2 mole fraction and $\Delta^{14}CO_2$ of about 30 ‰ (in 2014), the addition of 1 ppm of CO_{2ff} results in a decrease in $\Delta^{14}CO_2$ of ~2.7 ‰ (e.g., Turnbull et al. 2006). Current ^{14}C measurement uncertainties are, at best, just under 2 ‰ in ^{14}C, from both accelerator mass spectrometry (AMS) and gas counting methods (Graven et al. 2007; Turnbull et al. 2007; Levin et al. 2010). Since both Δ_{obs} and Δ_{bg} are used in calculating CO_{2ff}, the resulting uncertainty in CO_{2ff} due to measurement uncertainty alone is about ±1 ppm. Ongoing development of measurement techniques may bring the uncertainties down to 0.6–0.7 ppm in the near future.

Confounding influences, which are wrapped up in the second term in Eq. 4.7, can be important in some regions. This term can be regarded as the potential bias in CO_{2ff} if the non-fossil influences are not accounted for. Over the continents, heterotrophic respiration and biomass burning are the most important of these influences. In the tropics, and possibly at high northern latitudes, biospheric sources may have particularly substantial impacts on $^{14}CO_2$. In the tropics, the large magnitude of the respiration CO_2 flux means that even if the ^{14}C disequilibrium is small, the impact on $^{14}CO_2$ can be significant. At high latitudes, biospheric C may have resided in the soil for long periods, particularly if warming unlocks C that has been frozen for centuries or millennia (Chap. 6). This may result in a large and variable isotopic disequilibrium. The bias from biospheric sources on $^{14}CO_2$-derived estimates of CO_{2ff} has been estimated at 0.2–0.5 ppm over the Northern Hemisphere mid-latitudes and may be larger in the tropics and at high latitudes (Turnbull et al. 2009a). Since the bias is much smaller than typical ^{14}C measurement precision, some researchers have assumed it to be zero (e.g., Meijer et al. 1996; Levin et al. 2003).

Ethanol and other biofuels mixed with or replacing fossil gasoline may also need to be accounted for. In the ^{14}C method, these are not distinguishable from biomass burning or heterotrophic respiration fluxes. In contrast, other methods, particularly bottom-up inventory-based methods, may include biofuels in the gasoline budget. Some researchers have included biofuels in their ^{14}C-based CO_{2ff} estimates by measuring the ^{14}C of vehicle exhaust (Djuricin et al. 2010). Where biofuel content is known (e.g. mandated by government), adjusted ^{14}C of gasoline can also be calculated.

Another influence over continental regions arises from nuclear activities which produce ^{14}C from nuclear power generation and combustion or reprocessing of radioactive waste. The total ^{14}C isoflux from these activities is small relative to other sources, but the effect can be significant close to nuclear sites. For example, a study of fossil fuel emissions in Heidelberg, Germany, required an explicit correction of about 4.8 ‰ in $\Delta^{14}CO_2$ to account for the effects of a nearby nuclear reactor (Levin et al. 2003). A dataset of estimated $^{14}CO_2$ emissions from all known nuclear reactors is available (Graven and Gruber 2011) that takes into account varying ^{14}C emissions from different reactor types. For example, heavy water reactors used in Canada and gas-cooled reactors used in the UK emit much more ^{14}C for the same amount of electrical power generation than other reactor types. Most reactor types produce ^{14}C predominantly as $^{14}CO_2$, with the exception of pressurized water reactors, which produce ^{14}C predominantly as methane ($^{14}CH_4$). There is a lag time of several years before $^{14}CH_4$ is oxidized to $^{14}CO_2$, which affects where and when that $^{14}CO_2$ would be detected in atmospheric measurements. The magnitude and timing of nuclear reactor ^{14}C releases are imperfectly known, and there appears to be substantial variability in the amount of ^{14}C released even amongst reactors of the same type. Incineration of biomedical and other radioactive waste that contains ^{14}C in high concentrations is permitted to occur, but is poorly documented even though it can have a strong effect on local $^{14}CO_2$ measurements (e.g., Trumbore et al. 2002).

Over marine or coastal regions, a potential bias from ocean exchange may also be present. This is likely to be largest in areas close to upwelling regions in the Southern Ocean and the northwest Pacific Ocean where the isotopic disequilibrium between atmosphere and ocean is greatest (Randerson et al. 2002; Key et al. 2004; Turnbull et al. 2009a). For most continental regions of interest, this effect can be eliminated by careful choice of background, using a measurement station that reflects the same ocean influence as the region of interest.

Different sampling methods can be used to make the ^{14}C measurements. Flask samples are collected over a few minutes or up to one hour (Meijer et al. 1996; Turnbull et al. 2007; Graven et al. 2009; Djuricin et al. 2010; Turnbull et al. 2012) and can therefore be examined in the context of specific wind conditions and emission plumes. The same flask samples can be measured for other species to provide additional information (Turnbull et al. 2006; Miller et al. 2012). Integrated samples (either CO_2 absorbed into alkali, or plant material proxies) represent a longer term mixture of air masses and can be used to easily and cost-effectively examine broadscale gradients and long-term changes (Levin et al. 2008).

4.8.2 Large-Scale Spatial Fossil Fuel Carbon Dioxide Variability and Plant Material Proxies

Global $^{14}CO_2$ modeling studies (Randerson et al. 2002; Turnbull et al. 2009a; Miller et al. 2012) have been used to examine the spatial variability of $^{14}CO_2$ in the recent atmosphere. These models use best estimates of the ^{14}C isoflux magnitudes and spatial and temporal patterns to predict the atmospheric distribution of $^{14}CO_2$. They produce reasonable representations of the observed spatial distribution, although they do not resolve all the finer details, particularly at small scales. These global models have shown that $^{14}CO_2$ variability over the Northern Hemisphere land is dominated, at the continental scale (i.e., across a single continent), by CO_{2ff} emissions (Fig. 4.15).

On the observation side, plant materials have proven to be an excellent proxy for $^{14}CO_2$ at the continental, annual scale, allowing them to be used to understand the broad spatial distribution of $^{14}CO_2$ and to compare with model simulations. Since photosynthetic uptake does not alter ^{14}C, short-lived annual plants reflect atmospheric $^{14}CO_2$ averaged over their growing season, with the caveats that most plants

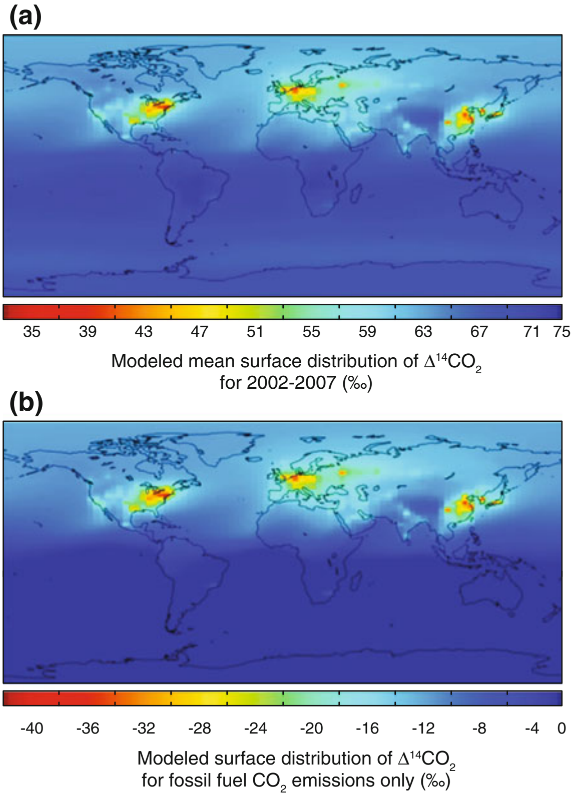

Fig. 4.15 (**a**) Modeled mean surface $\Delta^{14}CO_2$ distribution from the LMDZ model for 2002–2007. All known ^{14}C fluxes are included. (**b**) Modeled mean surface $\Delta^{14}CO_2$ distribution for 2002–2007 if fossil fuel CO_2 is the only source that alters $\Delta^{14}CO_2$ (i.e., no other sources are considered). The range of the two scales is the same (40 ‰). Figure modified from Turnbull et al. (2009b)

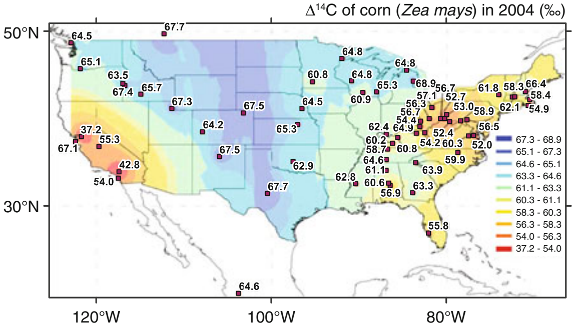

Fig. 4.16 Radiocarbon measurements of corn (*Zea mays*) across North America during the summer of 2004 (in units of ‰). *Squares* show actual measured values, and colors are the interpolated spatial distribution. During this time period, a decrease of 2.8 ‰ corresponded to ~1 ppm of added fossil fuel CO_2. Figure modified from Hsueh et al. (2007)

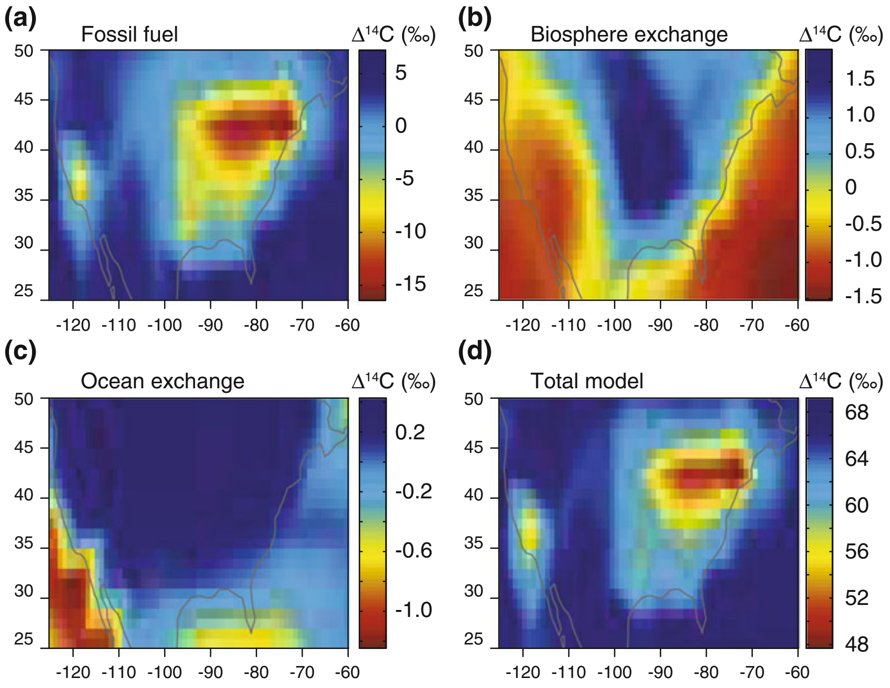

Fig. 4.17 Modeled contributions to surface atmospheric $\Delta^{14}C$ anomalies (with units of ‰) caused by (**a**) fossil fuel emissions, (**b**) terrestrial biosphere exchange, and (**c**) ocean exchange as derived from a global model during May–July of 2004 and (**d**) the combined influence of these processes, along with the effects of stratosphere–troposphere mixing. The background ^{14}C in (**d**) was adjusted by a single uniform scalar so that the mean of the model was the same as the mean of corn observations from western US mountains. Figure modified from Hsueh et al. (2007)

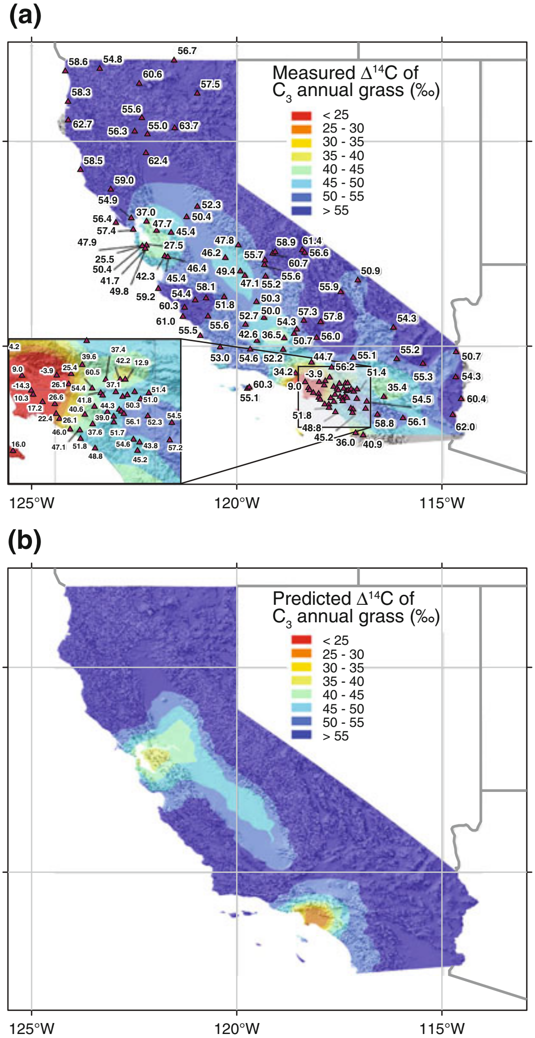

Fig. 4.18 Spatial pattern of $\Delta^{14}C$ from C_3 annual grasses in California, USA, from (**a**) observations in 2005 and (**b**) model simulation for annual grasses. In (**a**), *triangles* are actual observation sites, and *color scale* shows the interpolated spatial pattern. An expanded view of the Los Angeles area observations is shown on the *bottom left* of panel (**a**). Figures modified from Riley et al. (2008)

photosynthesize C only during the day, and that the magnitude of photosynthetic uptake varies with weather conditions and plant growth phase (Bozhinova et al. 2013). Two of the first studies used corn (maize) leaves and annual grasses to map ^{14}C across the USA and within California (Hsueh et al. 2007; Riley et al. 2008). The spatial pattern measured in corn across North America is broadly matched by models, with the lowest $\Delta^{14}CO_2$ values, indicative of strong CO_{2ff} sources, in the northeastern USA and on the California coast, and higher $\Delta^{14}CO_2$ values over the central region and Rocky Mountains (Figs. 4.16 and 4.17). In California, variations in the spatial distribution compared to model simulations show where model transport could be improved at the regional scale (Riley et al. 2008; Fig. 4.18). For example, the model used by Riley et al. (2008) predicts an area of low $\Delta^{14}CO_2$ values over Los Angeles. The observations reflect the same broad pattern, but show even lower values in Los Angeles, and also indicate an area of low $\Delta^{14}CO_2$ to the east of Los Angeles which is not predicted by the model.

Wine ethanol has also been used to map $^{14}CO_2$, and since wine vintages are rigorously documented, both the spatial distribution and the recent history of $^{14}CO_2$ can be obtained (Palstra et al. 2008). In Japan, ubiquitous rice grains provide similar spatial and historical $^{14}CO_2$ information (Shibata et al. 2005). In a study of rice, samples taken near the large number of nuclear power plants in Japan exhibited higher $\Delta^{14}CO_2$ values and were screened out to obtain the CO_{2ff} influence. In another study of large-scale ^{14}C patterns, flask samples of air were used to map $^{14}CO_2$ from a train-based platform across Eurasia (Turnbull et al. 2009b). Several of these samples were influenced by nearby nuclear power plant emissions. The nature of the near-instantaneous flask samples made it possible to screen out these samples to reveal the continental-scale $^{14}CO_2$ gradient, which was generally consistent with a modeled result.

4.8.3 Quantification of Fossil Fuel Carbon Dioxide Emissions at the Urban and Regional Scale

At the smaller scale, $^{14}CO_2$ is commonly used in urban regions to quantify fossil fuel emissions and to examine emissions of other anthropogenic trace gases. The method began to be used in a quantitative way in the late 1980s, with several studies calculating CO_{2ff} in flask samples of air from Europe (Levin et al. 1989; Meijer et al. 1996; Zondervan and Meijer 1996). Longer time series using CO_2 absorbed into alkali from German air followed (Levin et al. 2003, 2008). These measurements demonstrated large CO_{2ff} enhancements in the city of Heidelberg relative to clean-air sites (Fig. 4.19).

The $^{14}CO_2$ method has been shown to be less prone to biases than other tracer methods of quantifying CO_{2ff} (Turnbull et al. 2006; Djuricin et al. 2010; Fig. 4.20). However, the utility of the method is limited by two major factors. First, the accuracy of calculated CO_{2ff} is limited by the ^{14}C measurement precision. Second, the complex measurement techniques mean that samples must be transported and analyzed in a laboratory, limiting the temporal and spatial resolution of measurements. Therefore, ^{14}C measurements are often combined with other, more easily measured tracers to increase the resolution of CO_{2ff} estimates. The most widely used of the other tracers is CO, which is co-emitted with CO_2 during incomplete combustion. If the CO/CO_{2ff} emission ratio is known, CO_{2ff} can be calculated from CO measurements, but the emission ratio is variable depending on combustion conditions, and CO has other sources and sinks (Turnbull et al. 2006). These confounding problems can often be addressed by obtaining $^{14}CO_2$ and CO measurements from flasks or time-integrated samples (e.g., air collected in bags) to

Fig. 4.19 (**a**) Long-term $\Delta^{14}CO_2$ observations at Jungfraujoch; the smooth solid line is a harmonic fit to the monthly mean observations. (**b**) Monthly mean $\Delta^{14}CO_2$ at Schauinsland and Heidelberg. The *inlay* shows the comparison of observations at two different Heidelberg sites about 500 m apart. (**c**) Monthly mean fossil fuel CO_2 at Schauinsland calculated using Jungfraujoch as background. (**d**) Monthly mean fossil fuel CO_2 at Heidelberg using Jungfraujoch as background. Figure modified from Levin et al. (2008)

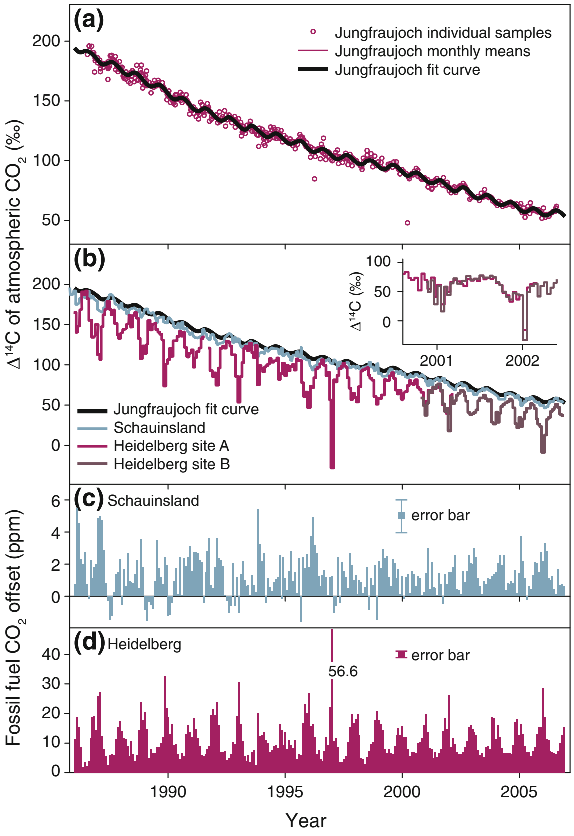

quantify the CO/CO_{2ff} ratio at a given location and time period. The derived emission ratio can then be used to obtain high-resolution CO_{2ff} from continuous CO measurements at the same location (Levin and Karstens 2007; Vogel et al. 2010; Turnbull et al. 2011).

These high-resolution CO_{2ff} estimates from combined CO and $^{14}CO_2$ measurements have been used in combination with estimates of atmospheric transport to determine the CO_{2ff} emission flux and compared with reported emission fluxes from bottom-up inventories. In these studies, the estimated emission fluxes have been reasonably consistent with reported inventory data, but have large uncertainties that are dominated not by the ^{14}C measurement uncertainty, but by uncertainties in the atmospheric transport of emissions. Turnbull et al. (2011) used a simple Gaussian plume model to describe atmospheric transport at the urban scale, but this type of model requires explicit knowledge of the wind speed and the planetary boundary layer height (emissions are assumed to mix within the planetary boundary layer, but not to escape into the free troposphere). The planetary boundary layer height in particular is difficult to represent in models and is the subject of

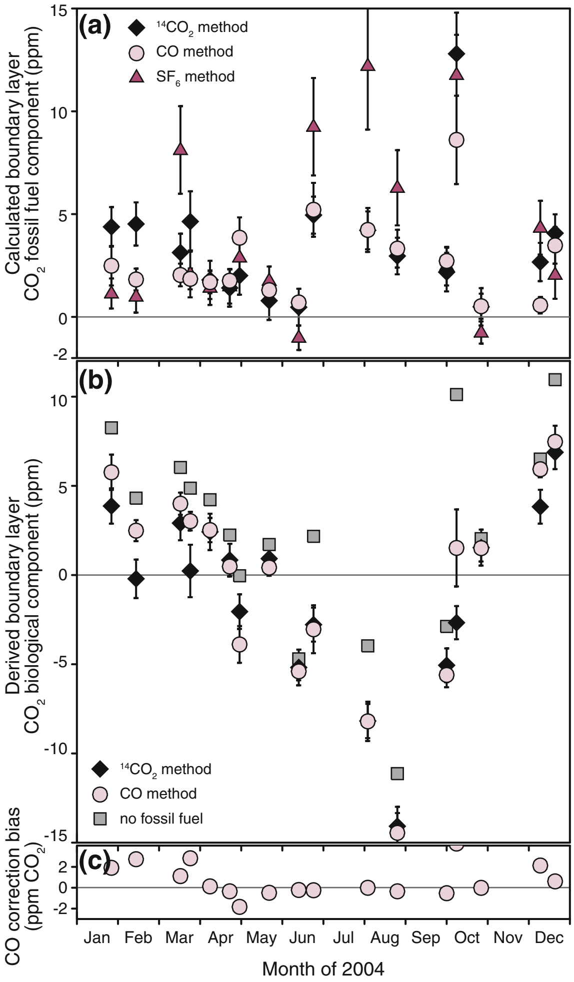

Fig. 4.20 (**a**) Calculated boundary layer fossil fuel CO_2 at Harvard Forest, USA, using $^{14}CO_2$ and the CO and SF_6 correlate tracer methods. (**b**) Derived boundary layer biological CO_2 component from total CO_2 and CO_{2ff} derived from each method. (**c**) Bias in the CO-derived CO_{2ff} relative to $^{14}CO_2$-dervied CO_{2ff}. Figure modified from Turnbull et al. (2006)

ongoing research. At even smaller scales such as single point source monitoring, averaging over long time periods may be needed to reduce uncertainties due to turbulent mixing and obtain reasonable agreement between model and observations (Turnbull et al. 2014). Van Der Laan et al. (2010) used a different approach, avoiding the need for explicit knowledge of the meteorological parameters by correlating their CO_{2ff} measurements with ^{222}Rn. ^{222}Rn is a gas produced by radioactive decay in the soil and released to the atmosphere. Its short half-life of a few days and relatively consistent emission across all land regions means that it is an excellent tracer for boundary layer stability and mixing. By assuming the ^{222}Rn emissions, and correlating CO_{2ff} with ^{222}Rn, it is possible to back-calculate the CO_{2ff} emissions. In this method, uncertainties in the ^{222}Rn emissions dominate.

4.8.4 Other Applications of Fossil Fuel Carbon Dioxide Measurements

Radiocarbon-derived CO_{2ff} estimates are also useful in quantifying CO_2 exchange with the terrestrial biosphere. Once the CO_{2ff} mole fraction is known, any remaining CO_2 variability over a land region must be ascribed to biological CO_2 exchange (including photosynthesis, respiration, biomass burning, and biofuel use). Contrary to initial expectations, CO_{2ff} is not always the dominant source of CO_2 variability even in highly urbanized regions, and respiration can be an important component, even in winter. A study in Los Angeles, California, USA, in 2007 and 2008, partitioned CO_2 sources using ^{14}C, ^{13}C, and ^{18}O. At a highly urbanized site, in a semi-arid environment, Djuricin and co-workers found that fossil fuel emissions contributed 30–50 % of the total CO_2 enhancement relative to background CO_2 values at Trinidad Head in Northern California and background $^{14}CO_2$ values at Point Barrow, Alaska (Djuricin et al. 2010; Fig. 4.21). In another study, the biosphere was shown to contribute up to 30 % of the total CO_2 enhancement in samples taken over Sacramento, California, in February and March 2009 (Turnbull et al. 2011). This study also found that the biosphere contribution could be different in sign between the urban area and the surrounding rural region. A third study over Denver, Colorado, USA, showed that respiration contributed 30–50 % of the total CO_2 enhancement in summer during the morning (Graven et al. 2009). All of these studies made measurements relative to continental clean-air or free troposphere background values. When more local background sites are used, it is likely that the

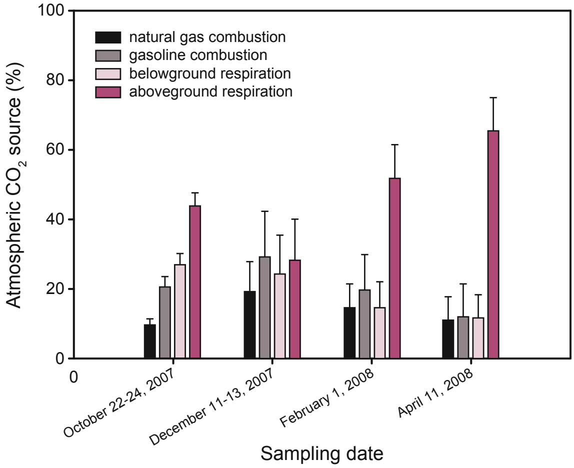

Fig. 4.21 Partitioning of CO_2 sources in Los Angeles, USA, for four episodes in 2007 and 2008. Sources were partitioned using $^{14}CO_2$ to obtain the fossil fraction, $^{13}CO_2$ to separate the different types of fossil fuel sources, and ^{18}O of CO_2 to identify the different types of respiration. Note also that bioethanol additive in gasoline was accounted for in the fossil fraction. Figure modified from Djuricin et al. (2010)

biosphere contribution in an urban area will appear much smaller, as much of the biosphere influence is likely coming from the surrounding countryside rather than the urban area itself.

The CO_{2ff} emission flux, while somewhat uncertain, is better known than fluxes of most other anthropogenic trace gases. The CO_{2ff} emission flux is known within 3–40 % at the annual, national scale, and within 20–50 % at regional and urban scales (Gurney et al. 2009; Marland 2010; Peylin et al. 2011). Fluxes of other species (e.g., hydrocarbons, halocarbons, criteria air pollutants) may be known to within only 50–100 % at the annual, national scale, and even more poorly at the urban and regional scales. The emission ratio of CO_{2ff} to another trace gas can therefore be used to improve the constraint on the flux of any trace gas with sources that are colocated with fossil fuel combustion. This ratio method avoids the need for atmospheric transport to be explicitly known or modeled. Meijer et al. (1996) pioneered this approach to examine CO emissions in the Netherlands, and other studies have since shown that bottom-up emission inventories of CO for much of the USA were too high (Turnbull et al. 2006; Graven et al. 2009; Miller et al. 2012), whereas observed CO/CO_{2ff} ratios were consistent with emission inventories for Germany and California (Vogel et al. 2010; Turnbull et al. 2011). The same method has also been used to evaluate hydrocarbon and halocarbon emissions in California (Turnbull et al. 2011) and the eastern USA (Miller et al. 2012).

4.8.5 Volcanic Carbon Dioxide Emissions

The volcanic CO_2 isoflux is very small compared to the other isofluxes and hence is ignored at the global and regional scales. Yet offsets in local atmospheric $^{14}CO_2$ are measurable in volcanic calderas and within 1 km of springs and seeps where there is outgassing of ^{14}C-free magmatic CO_2; this can be thought of as a natural analogue to the $^{14}CO_2$ depletion near cities and power plants where fossil fuel burning is concentrated. One of the first measurements of local $^{14}CO_2$ depletion attributable to volcanic activity was made on reeds and tree leaves at the shores of a lake in the volcanic Eifel region of western Germany with extensive CO_2 bubbling. Plants growing next to the lake showed $\Delta^{14}C$ decreases of ~100 ‰, but the depletion was undetectable ~100 m from the lake (Bruns et al. 1980). Other studies have shown that at the very local scale, $^{14}CO_2$ can be used as a sensitive tracer of CO_2 outgassing, just as it is a sensitive tracer of fossil fuel combustion at larger scales (Pasquier-Cardin et al. 1999; Saurer et al. 2003).

4.9 Atmospheric Radiocarbon in Other Compounds

4.9.1 ^{14}CO as a Detector for Hydroxyl Radicals

The isotope ^{14}CO tells a very different story about the atmosphere than $^{14}CO_2$. Produced naturally in the upper atmosphere, ^{14}C oxidizes extremely rapidly to ^{14}CO. The oxidation of ^{14}CO by hydroxyl radical (OH) to $^{14}CO_2$ occurs with a timescale of about two months (Weinstock and Niki 1972). Hydroxyl radicals provide the oxidizing power of the atmosphere, removing many important trace gases, including CH_4, CO, volatile organic compounds, and hydrochlorofluorocarbons. OH is produced naturally in the atmosphere during sunlit hours and its high reactivity means that it has a fleeting atmospheric lifetime of only a fraction of a second, making it extremely difficult to directly measure and study (Krol and Lelieveld 2003). OH might be expected to vary due to changes in its production and changes in the abundance of the trace gases which react with it. This variability in OH can have significant consequences for the global atmosphere. For example, lower OH production would result in a longer atmospheric lifetime for CH_4, a strong greenhouse gas (Kirschke et al. 2013). If the ^{14}C production rate is known, then measurements of ^{14}CO concentration provide a method to indirectly estimate OH abundance and variability via its effect on CO lifetime.

This method has been used to estimate short-term variations in OH of 10 % in the Southern Hemisphere high latitudes (Manning et al. 2005; Fig. 4.22), which are attributed to volcanic and biomass burning emissions. Hemispheric differences in OH abundance can also be tested with ^{14}CO (Jöckel and Brenninkmeijer 2002). The short lifetime and high-altitude source of ^{14}CO makes it more sensitive to OH concentrations at high altitudes and high latitudes than to OH concentrations at low altitudes and low latitudes (Krol et al. 2008). The distribution of ^{14}CO can additionally be used to test stratosphere–troposphere exchange in atmospheric models (Jöckel and Brenninkmeijer 2002).

4.9.2 Fossil Methane Source Identification

Methane, like CO_2, is a greenhouse gas with both natural and anthropogenic sources. Methane levels have increased from ~800 parts per billion (ppb) in the preindustrial era to 1800 ppb at present. The CH_4 budget is more complex than that of CO_2, with a plethora of sources, and unlike CO_2 it is oxidized in the atmosphere with a lifetime of about 10 years (Kirschke et al. 2013). The ^{14}C content of CH_4 is one way of elucidating the CH_4 budget. Fossil CH_4 sources are ^{14}C-free, whereas CH_4 produced from modern biomass by microorganisms (e.g., in rice paddies, termites, and cows) and fires has a ^{14}C content similar to that of the atmosphere. The fossil fraction can, in principle, be obtained in an analogous manner to CO_{2ff} (Townsend-Small et al. 2012). However, $^{14}CH_4$ from nuclear power generation

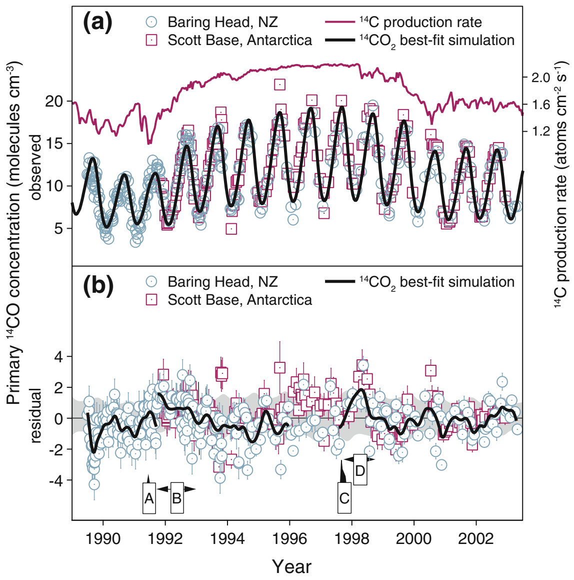

Fig. 4.22 (**a**) ^{14}CO concentrations for individual samples from Baring Head, New Zealand (*blue circles*) and Scott Base, Antarctica (*purple squares*) from 1989 to 2003. The *purple* and *black curves* show ^{14}C production rates (*right-hand scale*) and a best-fit simulation of ^{14}CO. (**b**) Residuals (observed minus simulated) for each measurement with uncertainties (1-sigma) and a smooth curve fit to the residuals (*black line*). The *gray shaded* regions show the deviations from the best fit that would be caused by a 10 % change in OH concentrations. *A*—time of eruption of Mt Pinatubo; *B*—period of high Southern Hemisphere CH_4 concentrations; *C*—time profile of Indonesian fires; *D*—period of high Southern Hemisphere CO concentrations. Figure modified from Manning et al. (2005)

comprises perhaps 20–40 % of the $^{14}CH_4$ budget (Quay et al. 1999), complicating the interpretation of $^{14}CH_4$ measurements. Nevertheless, observations and modeling have estimated the fossil CH_4 fraction from $^{14}CH_4$ measurements at ~30 % versus 20 % from bottom-up CH_4 emission inventories (Lassey et al. 2007).

A novel and challenging use of $^{14}CH_4$ measurements has been to identify the cause of the abrupt CH_4 increase from about 500 to over 700 parts per billion (ppb) during the Younger Dryas–Preboreal transition about 11,600 years ago (Petrenko et al. 2009; Fig. 4.23). Several mechanisms could have driven the CH_4 increase, with increased wetland CH_4 emissions and destabilization of marine CH_4 hydrate (solid CH_4 and water mixtures quite commonly found on the ocean floor) being the most likely. Tiny amounts of CH_4 were extracted from air bubbles in ~1000 kg of Greenland ice and measured for $^{14}CH_4$. Wetland $^{14}CH_4$ should be similar to that of the contemporaneous atmosphere, whereas CH_4 hydrate CH_4 was ancient and contained no ^{14}C. The measurements were confounded by in situ cosmogenic production of $^{14}CH_4$ molecules in the Arctic ice. After modeling cosmogenic production to remove this effect (which increased $\Delta^{14}CH_4$ by about

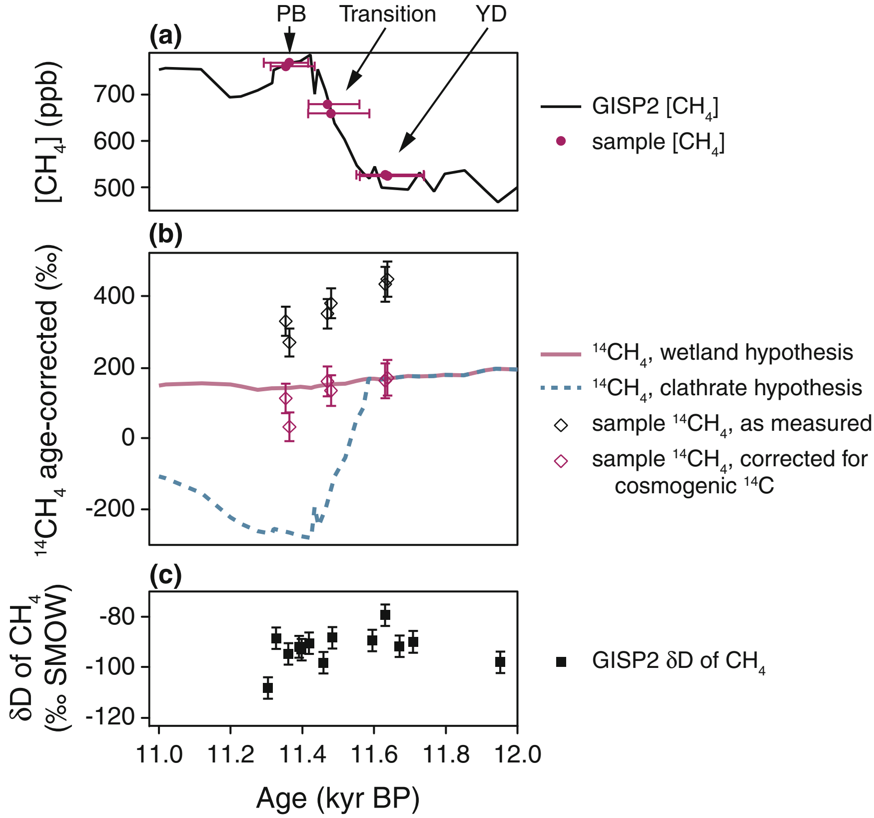

Fig. 4.23 $^{14}CH_4$ during the Younger Dryas (YD)—Preboreal (PB) transition. For the wetland hypothesis, 100 % biospheric CH_4 emissions are assumed for all times, with $^{14}CH_4$ equal to contemporaneous $^{14}CO_2$. For the CH_4 hydrate hypothesis, all of the CH_4 rise during the transition is assumed to be due to CH_4 hydrate emissions which decrease linearly to 0 over 1000 years, and have $^{14}CH_4$ of −1000 ‰. The transient $^{14}CH_4$ increase at 11.44 thousand years B.P. in the CH_4 hydrate model line corresponds to the simultaneous transient drop in CH_4 mole fraction. Horizontal error bars represent the maximum possible range of air ages. Figure modified from Petrenko et al. (2009)

200 ‰), the researchers found that $\Delta^{14}CH_4$ during the Younger Dryas—Preboreal transition stayed roughly constant at about 180 ‰. The CH_4 hydrate hypothesis predicts a decrease of $\Delta^{14}CH_4$ to about −200 ‰ during this period, so the CH_4 rise must have been due primarily to wetland sources, and not due to large-scale CH_4 hydrate destabilization.

4.9.3 Aerosol Source Attribution

Aerosols are another important area of atmospheric research, having both a climate effect and a negative impact on human health. As for other atmospheric trace species, understanding the sources is a critical part of the puzzle, and aerosol sources can be partitioned into fossil and biogenic components using ^{14}C measurements of the C in the aerosols.

Radiocarbon measurement can determine the fossil fuel contribution to total aerosol (or a collected size range) versus biogenic sources. Yet this misses an important part of the story, as anthropogenic biomass burning is also a substantial contributor to aerosols which cannot be distinguished from natural biogenic sources of aerosol. The elemental C (soot) fraction of aerosols is unique in being produced only as primary particles from fossil fuel combustion and biomass burning, whereas the organic C aerosol component is a mixture of primary sources including fossil fuel, biomass burning, and natural biogenic materials such as plant debris and pollen as well as secondary aerosol formed from gaseous precursors (Slater et al. 2002).

A study in Zurich, Switzerland, in 2002 and 2003 separated and measured both the soot and organic aerosol fractions (Szidat et al. 2006). The $\Delta^{14}C$ of the soot fraction ranged from less than −900 ‰ in summer to −750 ‰ in winter. They assigned a biomass burning $\Delta^{14}C$ of 240 ‰ in Zurich, assuming residential wood burning of 30- to 50-year-old wood, and fossil fuel $\Delta^{14}C$ of −1000 ‰. Using a simple two-member mixing model akin to the fossil fuel CO_2 method (Sect. 4.8), they determined that soot aerosol is produced solely by fossil fuel combustion in summer, but in winter, biomass burning contributes up to 25 %, even though biomass burning is only a tiny portion of local energy use. In contrast, organic aerosols had $\Delta^{14}C$ values of about −200 ‰ in all seasons of the year. This implies that the fossil fuel contribution was about 30 % of organic aerosol throughout the year. By assuming a consistent emission ratio of soot and organic biomass burning aerosols, they could further show that of the remaining non-fossil 70 % of organic aerosol, anthropogenic biomass burning was the main contributor in winter, but that natural biogenic sources became dominant in summer.

4.10 Conclusions and Future Directions

4.10.1 Improved Radiocarbon Measurement Techniques and Comparability

Atmospheric ^{14}C measurements are expanding to measure new trace gas species and to answer ever more detailed questions about our Earth System. A major limitation is the sample size requirement and difficulty of both AMS and decay counting measurement techniques. Currently, single sample AMS precision in

$\Delta^{14}CO_2$ is ±2 to ±5 ‰, with only a few laboratories able to achieve precision of ±2 ‰ or better. In comparison with other materials that are measured for ^{14}C, the analysis of atmospheric samples of CO_2 requires less sample handling, while the required level of precision is higher. Therefore, laboratories measuring $^{14}CO_2$ have initiated intercomparison activities specific to $^{14}CO_2$ (Miller et al. 2010, 2013; Graven et al. 2013; Turnbull et al. 2013), in addition to the routine ^{14}C intercomparison activities that use solid materials (e.g., Scott et al. 2007). The $^{14}CO_2$ intercomparison will identify any laboratory offsets specific to $^{14}CO_2$ with high precision and enable measurements from different laboratories to be merged. A further issue that needs to be addressed is the comparability of measurements of CO_2 from flask samples conducted by AMS to those of integrated CO_2 samples conducted by counting techniques. Addressing this issue will require measurement and interpretation of atmospheric variability that is captured in flask sampling but averaged over by continuous sampling.

As global $^{14}CO_2$ decreases and CO_2 mixing ratio increases through time, the sensitivity of $^{14}CO_2$ to CO_{2ff} is gradually decreasing, so that the same measurement precision will result in larger CO_{2ff} uncertainties. Incremental improvements in AMS precision can drive down this uncertainty and expand the CO_{2ff} detection capability. Measurement precision drops markedly with small sample sizes, particularly limiting the usefulness of ^{14}C measurements for the less abundant trace gases. Developments in measuring smaller sample sizes to better precision will open up many more possibilities for the use of ^{14}C in atmospheric studies.

Optical ^{14}C measurement techniques currently under development have the potential to revolutionize this field, particularly for $^{14}CO_2$, which could then be measured in situ at high resolution. Advances in laser technology mean that lasers can now be created with a very fine range of output wavelengths. The general principle is that a laser can be tuned to a specific wavelength where $^{14}CO_2$ absorption occurs. The amount of absorption of that laser light as it passes through air or concentrated CO_2 would determine the $^{14}CO_2$ content. The particular challenges for optical measurement of $^{14}CO_2$ arise from its very low abundance. First, broadening of nearby absorption lines of other gases, particularly $^{12}CO_2$ and $^{13}CO_2$, likely obscures many of the $^{14}CO_2$ absorption lines. Second, the low abundance will also mean that detection of absorption is difficult. Preconcentration of air into pure or at least much higher CO_2 concentration is needed, and the path length through the cell will need to be extremely long Galli et al. (2011). The initial results are promising, but much work remains to demonstrate reliable high precision on reasonably sized samples. It is likely that other similar methods will also be investigated over the next few years.

4.10.2 Developing Radiocarbon Observations into Policy-Relevant Fossil Fuel Carbon Dioxide Emission Estimates

The use of $^{14}CO_2$ has gradually been recognized as the best way to quantify CO_{2ff} from atmospheric observations. It may provide the only method for objectively verifying reported CO_{2ff} emissions. This will likely remain the most important, and expanding, field of atmospheric ^{14}C research for quite some time. To this end, observation networks will need to be expanded, the techniques for inferring CO_{2ff} emissions from the atmospheric observations will need to evolve, and a larger capacity for $^{14}CO_2$ measurements will be essential.

In order to provide relevant estimates of CO_{2ff} emissions, a reasonable target for $^{14}CO_2$ observation and modeling programs is to aim toward achieving uncertainties of roughly ±20 % in CO_{2ff} emissions. This level of uncertainty is similar to the differences in bottom-up inventories estimated by different groups for regions encompassing whole countries, groups of neighboring countries, or individual cities or states/provinces (Marland et al. 2006; Rayner et al. 2010; Peylin et al. 2011). Of course, this may underestimate the actual uncertainty because of shared biases due to the use by different groups of the same economic data and similar extrapolation techniques. In any case, this level of uncertainty is larger than the agreed-upon emission reductions for most nations that ratified the Kyoto Protocol (less than 10 %). Therefore, observational techniques using $^{14}CO_2$ are likely to be employed as a method for validating bottom-up inventories, rather than providing a precise top-down estimate of fossil fuel emissions that verifies that emission reductions have been achieved by an individual country.

Even accuracies of ±20 % in CO_{2ff} emissions will be challenging to achieve from atmospheric observations. Pacala et al. (2010) estimated the CO_{2ff} enrichment for several large urban regions to be 3–15 ppm, depending on the total emissions, population density, and meteorological characteristics of each city. This equates to a $\Delta^{14}CO_2$ decrease of −6 to −40 ‰. Continental-scale signals in $\Delta^{14}CO_2$ caused by regionally concentrated CO_{2ff} emissions are likely to be −5 to −20 ‰, as shown in Sect. 4.8.2 (e.g., Hsueh et al. 2007). Attaining ±20 % uncertainty in CO_{2ff} emissions will therefore require reducing the combined uncertainties in the measurement of $^{14}CO_2$, in the specification of non-fossil influences to $^{14}CO_2$, and in modeled transport from their present levels.

Understanding atmospheric transport is perhaps the most difficult problem in interpreting atmospheric $^{14}CO_2$ measurements. The methodology for quantifying CO_{2ff} mole fraction in atmospheric samples is now well established, but translating those atmospheric observations to emission fluxes is still challenging. Improvements in atmospheric transport models can potentially solve this problem by more accurately describing the transport of emissions to the observation site. Other approaches can reduce the reliance on atmospheric transport models. Levin et al. (2008) showed how long-term $^{14}CO_2$ measurements at a single site, paired with long-term observations at a mountaintop reference site, could be used to detect changes in emissions through time. This technique reduces the reliance on knowledge of atmospheric transport, assuming that interannual variations and trends in winds or boundary layer ventilation do not change the influential source regions or the dilution of surface emissions. In Sect. 4.8.3, we described how Van Der Laan et al. (2010) used ^{222}Rn to constrain planetary boundary layer mixing without the need for explicit transport models, although this method instead requires ^{222}Rn emissions to be well-known.

On the other hand, since the CO_{2ff} emission flux is arguably better known than that of any other species, $^{14}CO_2$ measurements have another potential use: to validate and improve atmospheric transport models. Combining $^{14}CO_2$ observations, particularly vertically resolved observations, with forward models that use bottom-up emission inventories as surface fluxes could identify model biases in the transport of emissions. Model-data evaluations using $^{14}CO_2$ are likely to be effective in regions with well-quantified bottom-up emissions, such as the USA (Gurney et al. 2009). Achieved improvements in model transport could then be employed in regions with less well-quantified emissions, such as Asia (Gregg et al. 2008).

Continued observations of $^{14}CO_2$ in background air are also needed. Such background observations provide information on fossil fuel emissions at global scales through the observation of the long-term trend or interhemispheric gradient of $^{14}CO_2$. Currently, uncertainties in the non-fossil contributions to the trend and gradient, primarily the oceanic contribution, limit the use of $^{14}CO_2$ to estimate global emissions (Levin et al. 2010). Improvements in quantifying non-fossil influences on background $^{14}CO_2$ could enable global-scale estimates of fossil fuel emissions to be achieved in the future.

4.10.3 Detection of Climate-Related Changes in Air–Land or Air–Ocean Carbon Exchanges

The feedback between anthropogenic climate change and the global C cycle represents one of the largest uncertainties in future projections of global warming (Jones et al. 2013). Several possible mechanisms have been proposed that would reduce the uptake of anthropogenic CO_2 or release currently stored C as the climate warms, thereby enhancing the accumulation of atmospheric CO_2 and the increase in surface temperatures in the future. However, the potential strength of these feedback mechanisms is not well understood. At least two of the proposed mechanisms would significantly perturb ^{14}C exchange with the atmosphere, so that observations of $^{14}CO_2$ may provide a method for detecting climate C feedbacks.

Thawing of arctic permafrost has the potential to release large amounts of long-sequestered C to the atmosphere in the form of CO_2 and CH_4. Since this C is likely to be old, $^{14}CO_2$ and $^{14}CH_4$ measurements could be used to quantify these releases through the observation of an anomalous negative isoflux in the northern high latitudes. The geographic separation should allow “old” permafrost emissions, concentrated in northern high latitudes, to be distinguished from fossil fuel emissions, concentrated in northern mid-latitudes. Coordinated observations of $^{14}CO_2$, $^{14}CH_4$, and other trace gases may further refine the separation of permafrost from fossil sources.

Climate change may also release old CO_2 from the deep ocean through enhancement in the wind-driven upwelling of the Southern Ocean, a process that has been proposed to have already begun, in part because of strengthening of Southern Hemisphere winds by stratospheric ozone depletion (Le Quere et al. 2007; Lovenduski et al. 2007). Enhanced upwelling of deep waters in the Southern Ocean causes an anomalous negative isoflux by exposing greater amounts of old water, containing older C, to the air. Observations of enhanced local gradients or trends in $^{14}CO_2$ over the Southern Ocean may therefore enable an anomalous CO_2 release to be quantified.

The centennial-scale variability in interhemispheric offset of atmospheric $^{14}CO_2$ (Hogg et al. 2002) also remains unexplained. Changes in ocean or atmospheric circulation have been suggested as causes (McCormac et al. 2002; Knox and McFadgen 2004), but whether the observed variations are consistent with what is known about ocean and atmosphere dynamics has not been evaluated.

The distribution of $^{14}CO_2$ in the atmosphere over the last few decades could provide more information on the ocean–atmosphere gas exchange velocity, particularly in the Southern Ocean (Krakauer et al. 2006). Most studies of ocean bomb ^{14}C uptake have used only seawater ^{14}C measurements to constrain ocean uptake, but measuring bomb ^{14}C in Southern Ocean water samples is particularly difficult because it is very dilute (Broecker et al. 1980; Peacock 2004; Levin et al. 2010). Several studies have shown that both the current rate of decline of atmospheric $^{14}CO_2$ and its gradient between the tropics and the Southern Ocean are sensitive to ocean–atmosphere gas exchange over the Southern Ocean, a process that is otherwise difficult to measure.

Radiocarbon provides an immensely powerful tool in understanding C-containing constituents of the atmosphere and their sources and variability. In the past atmosphere, ^{14}C measurements shed light on ocean C cycle processes as well as cosmic ray flux variability. Recent advances have made $^{14}CO_2$ measurements the tool of choice in constraining CO_{2ff} emissions in the modern atmosphere and potentially a key to understanding the fate of those emissions as they are taken up into the ocean.

References

Boden, T.A., G. Marland, and R.J. Andres. 2012. Global, regional, and national fossil-fuel CO_2 emissions. Carbon Dioxide Information Analysis Center, Oak Ridge National Laboratory, U.S. Department of Energy, Oak Ridge, Tenn., U.S.A.

Bozhinova, D., M. Combe, S.W.L. Palstra, H.A.J. Meijer, M.C. Krol, and W. Peters. 2013. The importance of crop growth modeling to interpret the $^{14}CO_2$ signature of annual plants. *Global Biogeochemical Cycles* 27: 792–803.

Braziunas, T.F., I.Y. Fung, and M. Stuiver. 1995. The preindustrial atmospheric $^{14}CO_2$ latitudinal gradient as related to exchanges among atmospheric, oceanic, and terrestrial reservoirs. *Global Biogeochemical Cycles* 9: 565–584.

Broecker, W.S., T.-H. Peng, and R. Engh. 1980. Modeling the carbon system. *Radiocarbon* 22: 565–598.

Broecker, W.S., T.-H. Peng, H. Ostlund, and M. Stuiver. 1985. The distribution of bomb radiocarbon in the ocean. *Journal of Geophysical Research* C4: 6953–6970.

Bruns, M., I. Levin, K.O. Munnich, M.W. Hubberten, and S. Fillipakis. 1980. Regional sources of volcanic carbon dioxide and their influence on C14 content of present-day plant material. *Radiocarbon* 22: 532–536.

Caldeira, K., G.H. Rau, and P.B. Duffy. 1998. Predicted net efflux of radiocarbon from the ocean and increase in atmospheric radiocarbon content. *Geophysical Research Letters* 25: 3811–3814.

Ciais, P., C.L. Sabine, G. Bala, L. Bopp, V. Brovkin, J.G. Canadell, A. Chabbra, R. DeFries, J. Galloway, M. Heimann, C. Jones, C. Le Quere, R. Mymeni, S. Piao, and P. Thornton. 2013. Carbon and other biogeochemical cycles. In T.F. Stocker, D. Qin, G.-K. Plattner, M. Tignor, S. Allen, J. Boschung, A. Nauels, Y. Xia, V. Bex, and P. M. Midgley, eds. Climate Change 2013: The Physical Science Basis. Contribution of Working Group I to the Fifth Assessment Report of the Intergovernmental Panel on Climate Change. Cambridge University Press, Cambridge, United Kingdom and New York, NY, USA.

Currie, K.I., G. Brailsford, S. Nichol, A. J. Gomez, R.J. Sparks, K.R. Lassey, and K. Riedel. 2011. Tropospheric $^{14}CO_2$ at Wellington, New Zealand: the world's longest record. *Biogeochemistry* 104: 5–22. doi:10.1007/s10533-009-9352-6

De Jong, A.F., and W.G. Mook. 1982. An anomalous Suess effect above Europe. *Nature* 298: 641–644.

Denning, A.S., M. Holzer, K.R. Gurney, M. Heimann, R.M. Law, P.J. Rayner, I.Y. Fung, S. Fan, S. Taguchi, P. Friedlingstein, Y. Balkanski, J. Taylor, M. Maiss, and I. Levin. 1999. Three-dimensional transport and concentration of SF_6 a model intercomparison study (TransCom 2). *Tellus* 51B: 266–297.

Djuricin, S., D.E. Pataki, and X. Xu. 2010. A comparison of tracer methods for quantifying CO_2 sources in an urban region. *Journal of Geophysical Research* 115.

Friedrich, M., S. Remmele, B. Kromer, J. Hofmann, M. Spurk, K.F. Kaiser, C. Orcel, and M. Küppers. 2004. The 12,460-year hohenheim oak and pine tree-ring chronology from Central Europe: A unique annual record for radiocarbon calibration and paleoenvironment reconstructions. *Radiocarbon* 46: 1111–1122.

Frost, T., and R.C. Upstill-Goddard. 1999. Air-sea gas exchange into the millennium: Progress and uncertainties. *Oceanography and Marine Biology* 37(37): 1–45.

Galli, I., S. Bartalini, S. Borri, P. Cancio, D. Mazzotti, P. De Natale, and G. Giusfredi. 2011. Molecular gas sensing below parts per trillion: Radiocarbon-dioxide optical detection. *Physical Review Letters* 107: 270802.

Graven, H.D., and N. Gruber. 2011. Continental-scale enrichment of atmospheric $14CO_2$ from the nuclear power industry: Potential impact on the estimation of fossil fuel-derived CO_2. *Atmospheric Chemistry and Physics* 11: 12339–12349.

Graven, H.D., T.P. Guilderson, and R.F. Keeling. 2007. Methods for high-precision ^{14}C AMS measurement of atmospheric CO_2 at LLNL. *Radiocarbon* 49: 349–356.

Graven, H.D., B.B. Stephens, T.P. Guilderson, T.L. Campos, D.S. Schimel, J.E. Campbell, and R. F. Keeling. 2009. Vertical profiles of biospheric and fossil fuel-derived CO_2 and fossil fuel CO_2:CO ratios from airborne measurements of $\Delta^{14}C$, CO_2 and CO above Colorado, USA. *Tellus B* 61: 536–546.

Graven, H.D., N. Gruber, R. Key, S. Khatiwala, and X. Giraud. 2012a. Changing controls on oceanic radiocarbon: new insights on shallow-to-deep ocean exchange and anthropogenic CO_2 uptake. *Journal of Geophysical Research* 117.

Graven, H.D., T.P. Guilderson, and R.F. Keeling. 2012b. Observations of radiocarbon in CO_2 at La Jolla, California, USA 1992–2007: analysis of the long-term trend. *Journal of Geophysical Research* 117.

Graven, H.D., T.P. Guilderson, and R.F. Keeling. 2012c. Observations of radiocarbon in CO_2 at seven global sampling sites in the scripps flask network: Analysis of spatial gradients and seasonal cycles. *Journal of Geophysical Research* 117.

Graven, H.D., X. Xu, T. Guilderson, R.F. Keeling, S.E. Trumbore, and S. Tyler. 2013. Comparison of independent $\Delta 14CO_2$ records at point barrow, Alaska. *Radiocarbon* 55: 1541–1545.

Gregg, J.S., R.J. Andres, and G. Marland. 2008. China: Emissions Pattern of the world leader in CO_2 emissions from fossil fuel consumption and cement production. *Geophysical Research Letters* 35.

Gurney, K.R., R.M. Law, A.S. Denning, P.J. Rayner, D. Baker, P. Bousquet, L. Bruhwiler, Y.-H. Chen, P. Ciais, S. Fan, I.Y. Fung, M. Gloor, M. Heimann, K. Higuchi, J. John, T. Maki, S. Maksyutov, K.A. Masarie, P. Peylin, M. Prather, B.C. Pak, J. Randerson, J.L. Sarmiento, S. Taguchi, T. Takahashi, and C.-W. Yuen. 2002. Towards robust regional estimates of CO_2 sources and sinks using atmospheric transport models. *Nature* 415: 626–630.

Gurney, K.R., D.L. Mendoza, Y. Zhou, M.L. Fischer, C.C. Miller, S. Geethakumar, and S. de la Rue du Can. 2009. High resolution fossil fuel combustion CO_2 emission fluxes for the United States. *Environmental Science and Technology* 43: 5535–5541.

Heimann, M., and E. Maier-Reimer. 1996. On the relations between the oceanic uptake of CO_2 and its carbon isotopes. *Global Biogeochemical Cycles* 10: 89–110.

Hesshaimer, V., and I. Levin. 2000. Revision of the stratospheric bomb $^{14}CO_2$ inventory. *Journal of Geophysical Research* 105: 11641–11658.

Hesshaimer, V., M. Heimann, and I. Levin. 1994. Radiocarbon evidence for a smaller oceanic carbon dioxide sink than previously believed. *Nature* 201–203.

Hogg, A., F. McCormac, T. Higham, P. Reimer, M. Baillie, and J. Palmer. 2002. High-precision radiocarbon measurements of contemporaneous tree-ring dated wood from the British Isles and New Zealand: A.D. 1850–1950. *Radiocarbon* 44: 633–640.

Hogg, A.G., C. Bronk Ramsey, C. Turney, and J. Palmer. 2009a. Bayesian evaluation of the Southern Hemisphere radiocarbon offset during the holocene. *Radiocarbon* 51: 1165–1176.

Hogg, A.G., J. Palmer, G. Boswijk, P. Reimer, and D. Brown. 2009b. Investigating the interhemispheric ^{14}C offset in the 1st millennium A.D. and assessment of laboratory bias and calibration errors. *Radiocarbon* 51: 1177–1186.

Holton, J.R., P.H. Haynes, M.E. McIntyre, A.R. Douglass, R.B. Rood, and L. Pfister. 1995. Stratosphere-troposphere exchange. *Reviews of Geophysics* 33: 403–439.

Houghton, R.A. 2008. Carbon flux to the atmosphere from land-use changes: 1850–2005. TRENDS: A compendium of data on global change. Carbon dioxide information analysis center, Oak Ridge National Laboratory, US Department of Energy, Oak Ridge, TN, USA.

Hsueh, D.Y., N.Y. Krakauer, J.T. Randerson, X. Xu, S.E. Trumbore, and J.R. Southon. 2007. Regional patterns of radiocarbon and fossil fuel-derived CO_2 in surface air across North America. *Geophysical Research Letters* 34: L02816.

Hua, Q., and M. Barbetti. 2004. Review of tropospheric bomb C-14 data for carbon cycle modeling and age calibration purposes. *Radiocarbon* 46: 1273–1298.

Hua, Q., and M. Barbetti. 2007. Influence of atmospheric circulation on regional (CO_2)-^{14}C differences. *Journal of Geophysical Research-Atmospheres* 112.

Hua, Q., M. Barbetti, U. Zoppi, D. Fink, M. Watanasak, and G. Jacobsen. 2004. Radiocarbon in tropical tree rings during the little ice age. *Nuclear Instruments and Methods in Physics Research Section B-Beam Interactions With Materials and Atoms* 223: 489–494.

Hua, Q., M. Barbetti, D. Fink, K.F. Kaiser, M. Friedrich, B. Kromer, V.A. Levchenko, U. Zoppi, A.M. Smith, and F. Bertuch. 2009. Atmospheric C-14 variations derived from tree rings during the early younger dryas. *Quaternary Science Reviews* 28: 2982–2990.

Hua, Q., M. Barbetti, and A.Z. Rakowski. 2013. Atmospheric radiocarbon for the period 1950–2010. *Radiocarbon* 55: 2059–2072.

Hughen, K., S. Lehman, J. Southon, J. Overpeck, O. Marchal, C. Herring, and J. Turnbull. 2004. C-14 activity and global carbon cycle changes over the past 50,000 years. *Science* 303: 202–207.

Jacob, D.J. 1999. *Introduction to atmospheric chemistry*. Princeton, NJ, USA: Princeton University Press.

Johnston, C.A. 1994. Ecological engineering of wetlands by beavers. In *Global Wetlands: Old World and New*, ed. W.J. Mitsch, 379–384. Amsterdam: Elsevier.

Jones, C., E. Robertson, V. Arora, P. Friedlingstein, E. Shevliakova, L. Bopp, V. Brovkin, T. Hajima, E. Kato, M. Kawamiya, S. Liddicoat, K. Lindsay, C.H. Reick, C. Roelandt, J. Segschneider, and J. Tjiputra. 2013. Twenty-first-century compatible CO_2 emissions and airborne fraction simulated by CMIP5 earth system models under four representative concentration pathways. *Journal of Climate*, 26: 4398–4413.

Jöckel, P., M.G. Lawrence, and C.A.M. Brenninkmeijer. 1999. Simulations of cosmogenic ^{14}CO using the three-dimensional atmospheric transport model MATCH: Effects of ^{14}C production distribution and the solar cycle. *Journal of Geophysical Research*, 104(D9): 11733–11743.

Jöckel, P., and C.A.M. Brenninkmeijer. 2002. the seasonal cycle of cosmogenic ^{14}CO at the surface level: A solar cycle adjusted, zonal-average climatology based on observations. *Journal of Geophysical Research* 107: 4656.

Keeling, C.D., and T. Whorf. 2005. Atmospheric CO_2 records from sites in the SIO air sampling network. Trends: A compendium of data of global change. Carbon Dioxide Information Analysis Center, Oak Ridge National Laboratory, Oak RIdge, Tenn., USA.

Key, R.M., A. Kozyr, C.L. Sabine, K. Lee, R. Wanninkhof, J.L. Bullister, R.A. Feely, F.J. Millero, C. Mordy, and T.H. Peng. 2004. A global ocean carbon climatology: results from global data analysis project (GLODAP). *Global Biogeochemical Cycles* 18(4). doi:10.1029/2004gb002247(4).

Kirschke, S., P. Bousquet1, P. Ciais, M. Saunois, J.G. Canadell, E.J. Dlugokencky, P. Bergamaschi, D. Bergmann, D.R. Blake, L. Bruhwiler, P. Cameron-Smith, S. Castaldi, F. D.R. Chevallier, L. Feng, A. Fraser, M. Heimann, E.L. Hodson, A. Houweling, B.A. Josse, P. J. Fraser, P.B. Krummel, J.-F.O. Lamarque, R.L. Langenfelds, C.L. Quéré, V. Naik, S. O'Doherty, P.I. Palmer, I. Pison, D. Plummer, B. Poulter, R.G. Prinn, M. Rigby, B. Ringeval, M. Santini, M. Schmidt, D.T. Shindell, I.J. Simpson, R. Spahni, L.P. Steele, S.A. Strode, K. Sudo, S. Szopa, G. R.V.D. Werf, A. Voulgarakis, M.V. Weele, R.F. Weiss, J.E. Williams, and G. Zeng. 2013. Three decades of global methane sources and sinks. *Nature Geoscience* 6: 813–823.

Kitigawa, H., H. Mukai, Y. Nojiri, Y. Shibata, T. Kobayashi, and T. Nojiri. 2004. Seasonal and secular variations of atmospheric $^{14}CO_2$ over the Western Pacific since 1994. *Radiocarbon* 46: 901–910.

Kjellstrom, E., J. Feichter, and G. Hoffman. 2000. Transport of SF_6 and (CO2)-C^{14} in the atmospheric general circulation model ECHAM4. *Tellus Series B-Chemical and Physical Meteorology* 52: 1–18.

Knox, F., and B. McFadgen. 2004. Radiocarbon/tree ring calibration, solar activity, and upwelling of ocean water. *Radiocarbon* 46: 987–995.

Kohler, P., R. Muscheler, and H. Fischer. 2006. A model-based interpretation of low-frequency changes in the carbon cycle during the last 120,000 years and its implications for the reconstruction of atmospheric delta C-14. *Geochemistry Geophysics Geosystems* 7.

Krakauer, N., J. Randerson, F. Primeau, N. Gruber, and D. Menemenlis. 2006. Carbon isotope evidence for the latitudinal distribution and wind speed dependence of the air-sea gas transfer velocity. *Tellus Series B-Chemical and Physical Meteorology* 58: 390–417.

Krol, M.C., and J. Lelieveld. 2003. Can the variability in tropospheric OH be deduced from measurements of 1,1,1-trichloroethane (methyl chloroform)? *Journal of Geophysical Research* D108.

Krol, M.C., J.F. Meirink, P. Bergamaschi, J.E. Mak, D. Lowe, P. Jockel, S. Houweling, and T. Rockmann. 2008. What can ^{14}CO measurements tell us about OH? *Atmospheric Chemistry and Physics* 8: 5033–5044.

Kuc, T., K. Rozanski, M. Zimnoch, J. Necki, L. Chmura, and D. Jelen. 2007. Two decades of regular observations of $^{14}CO_2$ and $^{13}CO_2$ content in atmospheric carbon dioxide in central europe: long-term changes of regional anthropogenic fossil CO_2 emissions. *Radiocarbon* 49: 807–816.

Lal, D. 1988. Theoretically expected variations in the terrestrial cosmic-ray production rates of isotopes. In: Proceedings of the International school of Physics, Solar-Terrestrial Relationships and the Earth Environment in the Last Millennia, pp. 215–233.

Lal, D., and Rama. 1966. Characteristics of global tropospheric mixing based on man-made C14 H3 and Sr90. *Journal of Geophysical Research* 71: 2865.

Land, C., J. Feichter, and R. Sausen. 2002. Impact of vertical resolution on the transport of passive tracers in the ECHAM4 model. *Tellus B* 54: 344–360.

Lassey, K.R., D.C. Lowe, and A.M. Smith. 2007. The atmospheric cycling of radiomethane and the “fossil fraction” of the methane source. *Atmospheric Chemistry and Physics* 7: 2141–2149.

Le Quere, C., C. Rodenbeck, E.T. Buitenhuis, T.J. Conway, R. Langenfelds, A. Gomez, C. Labuschagne, M. Ramonet, T. Nakazawa, N. Metzl, N. Gillett, and M. Heimann. 2007. Saturation of the southern ocean CO_2 sink due to recent climate change. *Science* 316: 1735–1738.

Lerman, J.C., W.G. Mook, and J.C. Vogel. 1970. C-14 in tree rings from different localities. Radiocarbon variations and absolute chronology. In: Proceedings of the Twelfth Nobel Symposium held at the Institute of Physics at Uppsala University. Wiley Interscience Division, New York.

Levin, I., R. Boesinger, G. Bonani, R.J. Francey, B. Kromer, K.O. Muennich, M. Suter, N.B. A. Trivett, and W. Wolfli. 1992. Radiocarbon in atmospheric carbon dioxide and methane global distribution and trends. In: Taylor, R.E., A. Long and R. S. Kra eds. Radiocarbon After Four Decades: An Interdisciplinary Perspective; Meeting, Lake Arrowhead, California, USA, 4–8 June 1990. Xviii + 596 p. New York, USA; Berlin, Germany: Springer. Illus: 503–518.

Levin, I., and V. Hesshaimer. 2000. Radiocarbon: A unique tracer of global carbon cycle dynamics. *Radiocarbon* 42: 69–80.

Levin, I., and U. Karstens. 2007. Inferring high-resolution fossil fuel CO_2 records at continental sites from combined $^{14}CO_2$ and CO observations. *Tellus* 59B: 245–250.

Levin, I., and B. Kromer. 2004. The tropospheric $^{14}CO_2$ level in mid-latitudes of the Northern Hemisphere (1959–2003). *Radiocarbon* 46: 1261–1272.

Levin, I., J. Schuchard, B. Kromer, and K.O. Munnich. 1989. The continental European Suess effect. *Radiocarbon* 31: 431–440.

Levin, I., B. Kromer, M. Schmidt, and H. Sartorius. 2003. A novel approach for independent budgeting of fossil fuel CO_2 over Europe by $^{14}CO_2$ observations. *Geophysical Research Letters* 30: 2194.

Levin, I., S. Hammer, B. Kromer, and F. Meinhardt. 2008. Radiocarbon observations in atmospheric CO_2: determining fossil fuel CO_2 over Europe using Jungfraujoch observations as background. *Science of the Total Environment* 391: 211–216.

Levin, I., T. Naegler, B. Kromer, M. Diehl, R.J. Francey, A.J. Gomez-Pelaez, L.P. Steele, D. Wagenbach, R. Weller, and D.E. Worthy. 2010. Observations and modelling of the global distribution and long-term trend of atmospheric $^{14}CO_2$. *Tellus B* 62: 26–46.

Lovenduski, N.S., N. Gruber, S.C. Doney, and I.D. Lima. 2007. Enhanced CO_2 outgassing in the southern ocean from a positive phase of the southern annular mode. *Global Biogeochemical Cycles* 21.

Manning, M.R., D.C. Lowe, W.H. Melhuish, R.J. Sparks, G. Wallace, C.A.M. Brenninkmeijer, and R.C. McGill. 1990. The use of radiocarbon measurements in atmospheric sciences. *Radiocarbon* 32: 37–58.

Manning, M.R., D.C. Lowe, R.C. Moss, G.E. Bodeker, and W. Allan. 2005. Short-term variations in the oxidizing power of the atmosphere. *Nature* 436: 1001–1004.

Marland, G. 2010. Accounting for carbon dioxide emissions from bioenergy systems. *Journal of Industrial Ecology* 14: 866–869.

Marland, G., T.A. Boden, and R.J. Andres. 2006. Global, regional and national CO_2 emissions. Trends: A compedium of data on global change. Carbon Dioxide Information Analysis Center, Oak Ridge National Laboratory, US Department of Energy, Oak Ridge, TN.

Masarik, J., and J. Beer. 1999. Simulation of particle fluxes and cosmogenic nuclide production in the earth's atmosphere. *Journal of Geophysical Research-Atmospheres* 104: 12099–12111.

Mazaud, A., C. Laj, E. Bard, M. Arnold, and E. Tric. 1991. Geomagnetic-field control of C-14 production over the Last 80 Ky—Implications for the radiocarbon timescale. *Geophysical Research Letters* 18: 1885–1888.

McCormac, F., A. Hogg, T. Higham, J. Lynch-Stieglitz, W. Broecker, M. Baillie, J. Palmer, L. Xiong, J. Pilcher, D. Brown, and S. Hoper. 1998. Temporal variation in the interhemispheric C-14 Offset. *Geophysical Research Letters* 25: 1321–1324.

McCormac, F., P. Reimer, A. Hogg, T. Higham, M. Baillie, J. Palmer, and M. Stuiver. 2002. Calibration of the radiocarbon time scale for the Southern Hemisphere: A.D. 1850–1950. *Radiocarbon* 44: 641–651.

Meijer, H.A.J., H.M. Smid, E. Perez, and M.G. Keizer. 1996. Isotopic characterization of anthropogenic CO_2 emissions using isotopic and radiocarbon analysis. *Physical Chemistry of the Earth* 21: 483–487.

Miller, J.B., C. Wolak, S.J. Lehman, C.E. Allison, H.D. Graven, T.P. Guilderson, R.F. Keeling, H. A.J. Meijer, T. Nakamura, T. Nakazawa, R.E. Neubert, A.M. Smith, J.R. Southon, and X. Xu. 2010. Preliminary results of from the first intercomparison of accelerator mass spectrometry atmospheric $^{14}CO_2$ measurements. In: W. Brand, ed. 15th WMO/IAEA Meeting of Experts on Carbon Dioxide Concentration and Related Measurement Techniques. World Meteorological Organization, Geneva.

Meijer, H.A.J., M.H. Pertuisot, and J. van der Plicht. 2006. High-Accuracy C-14 measurements for atmospheric CO_2 samples by AMS. *Radiocarbon* 48: 355–372.

Miller, J.B., S.J. Lehman, S.A. Montzka, C. Sweeney, B.R. Miller, C. Wolak, E.J. Dlugokencky, J. R. Southon, J.C. Turnbull, and P.P. Tans. 2012. Linking emissions of fossil fuel CO_2 and other anthropogenic trace gases using atmospheric $^{14}CO_2$. *Journal of Geophysical Research* 117.

Miller, J.B., S. Lehmann, C. Wolak, J. Turnbull, G. Dunn, H. Graven, R. Keeling, H.A.J. Meijer, A.T. Aerts-Bijma, S.W.L. Palstra, A.M. Smith, C. Allison, J. Southon, X. Xu, T. Nakazawa, S. Aoki, T. Nakamura, T. Guilderson, B. LaFranchi, H. Mukai, Y. Terao, M. Uchida, and M. Kondo. 2013. Initial results of an intercomparison of AMS-based atmospheric $^{14}CO_2$ measurements. *Radiocarbon* 55: 1475–1483.

Muscheler, R., J. Beer, G. Wagner, C. Laj, C. Kissel, G. Raisbeck, F. Yiou, and P. Kubik. 2004. Changes in the carbon cycle during the last deglaciation as indicated by the comparison of ^{10}Be and ^{14}C records. *Earth and Planetary Science Letters* 219: 325–340.

Naegler, T., and I. Levin. 2006. Closing the global radiocarbon budget 1945–2005. *Journal of Geophysical Research-Atmospheres* 111.

Naegler, T., and I. Levin. 2009a. Biosphere-atmosphere gross carbon exchange flux and the delta (CO_2)-^{13}C and Delta(CO_2)-^{14}C disequilibria constrained by the biospheric excess radiocarbon inventory. *Journal of Geophysical Research-Atmospheres* 114.

Naegler, T., and I. Levin. 2009b. Observation-based global biospheric excess radiocarbon inventory 1963–2005. *Journal of Geophysical Research* 114.

Nakamura, T., T. Nakazawa, H. Honda, H. Kitagawa, T. Machida, A. Ikeda, and E. Matsumoto. 1994. Seasonal variations in ^{14}C concentrations of stratospheric CO_2 measured with accelerator mass spectrometry. *Nuclear Instruments and Methods* B92: 413–416.

Nakamura, T., T. Nakazawa, N. Nakai, H. Kitigawa, H. Honda, T. Itoh, T. Machida, and E. Matsumoto. 1992. Measurement of ^{14}C concentrations of stratospheric CO_2 by accelerator mass spectrometry. *Radiocarbon* 34: 745–752.

Nydal, R. 1963. Increase in radiocarbon from most recent series of thermonuclear tests. *Nature* 200: 212.

Nydal, R. 1968. Further investigation on transfer of radiocarbon in nature. *Journal of Geophysical Research* 73: 3617.

Nydal, R., and K. Lovseth. 1965. Distribution of Radiocarbon from Nuclear Tests. *Nature* 206: 1029.

Nydal, R., and K. Lovseth. 1983. Tracing bomb ^{14}C in the atmosphere 1962–1980. *Journal of Geophysical Research-Oceans and Atmospheres* 88: 3621–3642.

O'Brien, K. 1979. Secular variations in the production of cosmogenic isotopes in the earth's atmosphere. *Journal of Paleolimnology* 84: 423.

Oeschger, H., U. Siegenthaler, U. Schotterer, and A. Gugelmann. 1975. A box diffusion model to study the carbon dioxide exchange in nature. *Tellus* XXVII:168–192.

Pacala, S.W., C. Breidenich, P.G. Brewer, I.Y. Fung, M.R. Gunson, G. Heddle, B.E. Law, G. Marland, K. Paustian, M. Prather, J.T. Randerson, P.P. Tans, and S.C. Wofsy. 2010. *Verifying greenhouse gas emissions: methods to support international climate agreements*. Committee on Methods for Estimating Greenhouse Gas Emissions: National Research Council.

Palstra, S.W., U. Karstens, H.-J. Streurman, and H.A.J. Meijer. 2008. Wine ethanol ^{14}C as a tracer for fossil fuel CO_2 emissions in Europe: Measurements and model comparison. *Journal of Geophysical Research* 113.

Pasquier-Cardin, A., P. Allard, T. Ferreira, E.C. Hatt, R. Coutinho, M. Fontugne, and M. Jaudon. 1999. Magma derived CO_2 emissions recorded in ^{14}C and ^{13}C content of plants growing in furnas caldera, Azores. *Journal of Volcanology and Geothermal Research* 92: 195–207.

Peacock, S. 2004. Debate over the ocean bomb radiocarbon sink: Closing the gap. *Global Biogeochemical Cycles* 18.

Petrenko, V.V., A.M. Smith, E.J. Brook, D.C. Lowe, K. Riedel, G. Brailsford, Q. Hua, H. Schaefer, N. Reeh, R.F. Weiss, D.M. Etheridge, and J.P. Severinghaus. 2009. $^{14}CH_4$ measurements in greenland ice: Investigating the last glacial termination CH_4 sources. *Science* 324: 506–508.

Peylin, P., S. Houweling, M. Krol, U. Karstens, C. Rodenbeck, C. Geels, A. Vermeulen, B. Badawy, C. Aulagnier, T. Pregger, F. Delage, G. Pieterse, P. Ciais, and M. Heimann. 2011. Importance of fossil fuel emission uncertainties over Europe for CO_2 modeling: Model intercomparison. *Atmospheric Chemistry and Physics* 11: 6607–6622.

Quay, P.D., J. Stutsman, D. Wilbur, A.K. Snover, E.J. Dlugokencky, and T.A. Brown. 1999. The isotopic composition of atmospheric methane. *Global Biogeochemical Cycles* 13: 445–461.

Rafter, T.A., and G.J. Fergusson. 1957. "Atom bomb effect"—Recent increase of carbon-14 content of the atmosphere and biosphere. *Science* 126: 557–558.

Randerson, J., I. Enting, E. Schuur, K. Caldeira, and I. Fung. 2002. Seasonal and Latitudinal variability of troposphere $\Delta(CO_2)$-^{14}C: Post bomb contributions from fossil fuels, oceans, the stratosphere, and the terrestrial biosphere. *Global Biogeochemical Cycles* 16.

Rayner, P.J., M.R. Raupach, M. Paget, P. Peylin, and E. Koffi. 2010. A new global gridded data set of CO_2 emissions from fossil fuel combustion: Methodology and evaluation. *Journal of Geophysical Research* 115: D19306.

Reimer, P.J. 2013. IntCal13 and marine13 radiocarbon age calibration curves 0–50,000 years CAL BP. *Radiocarbon* 55: 1869–1887.

Reimer, P.J., M.G.L. Baillie, E. Bard, A. Bayliss, J.W. Beck, P.G. Blackwell, C.B. Ramsey, C.E. Buck, G.S. Burr, R.L. Edwards, M. Friedrich, P.M. Grootes, T.P. Guilderson, I. Hajdas, T. J. Heaton, A.G. Hogg, K.A. Hughen, K.F. Kaiser, B. Kromer, F.G. McCormac, S.W. Manning, R.W. Reimer, D.A. Richards, J.R. Southon, S. Talamo, C.S.M. Turney, J. van der Plicht, and C.E. Weyhenmeye. 2009. IntCal09 and marine09 radiocarbon age calibration curves, 0–50,000 years CAL BP. *Radiocarbon* 51: 1111–1150.

Revelle, R., and H.E. Suess. 1957. Carbon dioxide exchange between atmosphere and ocean and the question of an increase of atmospheric CO_2 during the past decades. *Tellus* 9: 18–27.

Riley, W.G., D.Y. Hsueh, J.T. Randerson, M.L. Fischer, J. Hatch, D.E. Pataki, W. Wang, and M. L. Goulden. 2008. Where do fossil fuel carbon dioxide emissions from California go? An analysis based on radiocarbon observations and an atmospheric transport model. *Journal of Geophysical Research* 113.

Rodgers, K.B., S.E. Mikaloff-Fletcher, D. Bianchi, C. Beaulieu, E.D. Galbraith, A. Gnanadesikan, A.G. Hogg, D. Iudicone, B.R. Lintner, T. Naegler, P.J. Reimer, J.L. Sarmiento, and R.D. Slater. 2011. Interhemispheric gradient of atmospheric radiocarbon reveals natural variability of southern ocean winds. *Climate of the Past* 7: 1123–1138.

Saurer, M., P. Cherubini, G. Bonani, and R. Siegwolf. 2003. Tracing carbon uptake from a natural CO2 spring into tree rings: An isotope approach. *Tree Physiology* 23: 997–1004.

Schuur, E.A.G., et al. 2015. Climate change and the permafrost carbon feedback. *Nature*, 520 (7546): 171–179, doi:10.1038/nature14338

Scott, E.M., G.T. Cook, P. Naysmith, C. Bryant, and D. O'Donnell. 2007. A report on phase 1 of the 5th international radiocarbon intercomparison (VIRI). *Radiocarbon* 49: 409–426.

Shibata, S., E. Kawano, and T. Nakabayashi. 2005. Atmospheric $[^{14}C]CO_2$ variations in Japan during 1982–1999 based on ^{14}C measurements of rice grains. *Applied Radiation and Isotopes* 63: 285–290.

Slater, J., L.A. Currie, J. Dibb, and B.A.J. Benner. 2002. Distinguishing the relative contribution of fossil fuel and biomass combustion aerosols deposited at summit, greenland through isotopic and molecular characterization of insoluble carbon. *Atmospheric Environment* 36: 4463–4477.

Stephens, B., K. Gurney, P. Tans, C. Sweeney, W. Peters, L. Bruhwiler, P. Ciais, M. Ramonet, P. Bousquet, T. Nakazawa, S. Aoki, T. Machida, G. Inoue, N. Vinnichenko, J. Lloyd, A. Jordan, M. Heimann, O. Shibistova, R. Langenfelds, L. Steele, R. Francey, and A. Denning. 2007. Weak northern and strong tropical land carbon uptake from vertical profiles of atmospheric CO_2. *Science* 316: 1732–1735.

Stuiver, M., and T.F. Braziunas. 1993. Sun, ocean, climate and atmospheric $^{14}CO_2$: An evaluation of causal and spectral relationships. *Holocene* 3: 289–305.

Stuiver, M., and T.F. Braziunas. 1998. Anthropogenic and solar components of hemispheric ^{14}C. *Geophysical Research Letters* 25: 329–332.

Stuiver, M., and P.D. Quay. 1981. Atmospheric ^{14}C changes resulting from fossil-fuel CO_2 release and cosmic-ray flux variability. *Earth and Planetary Science Letters* 53: 349–362.

Suess, H.E. 1955. Radiocarbon concentration in modern wood. *Science* 122: 415–417.

Sweeney, C., E. Gloor, A. Jacobson, R. Key, G. McKinley, J. Sarmiento, and R. Wanninkhof. 2007. Constraining global air-sea gas exchange for CO_2 with recent bomb ^{14}C measurements. *Global Biogeochemical Cycles* 21.

Szidat, S., T.M. Jenk, H.-A. Synal, M. Kalberer, L. Wacker, I. Hajdas, A. Kasper-Giebl, and U. Baltensperger. 2006. Contributions of fossil fuel, biomass-burning, and biogenic emissions to carbonaceous aerosols in zurich as traced by ^{14}C. *Journal of Geophysical Research* 111.

Takahashi, T., S.C. Sutherland, R. Wanninkhof, C. Sweeney, R.A. Feely, D.W. Chipman, B. Hales, G. Friederich, F. Chavez, C. Sabine, A. Watson, D.C.E. Bakker, U. Schuster, N. Metzl, H. Yoshikawa-Inoue, M. Ishii, T. Midorikawa, Y. Nojiri, A. Kortzinger, T. Steinhoff, M. Hoppema, J. Olafsson, T.S. Arnarson, B. Tilbrook, T. Johannessen, A. Olsen, R. Bellerby, C.S. Wong, B. Delille, N.R. Bates, and H.J.W. de Baar. 2009. Climatological mean and decadal change in surface ocean pCO_2, and net sea-air CO_2 flux over the global oceans. *Deep-Sea Research Part I-Oceanographic Research Papers* 56: 554.

Tans, P.P., A.F. De Jong, and W.G. Mook. 1979. Natural atmospheric ^{14}C variation and the Suess effect. *Nature* 280: 826–828.

Telegadas, K. 1971. The seasonal atmospheric distribution and inventories of excess ^{14}C from March 1955 to July 1969. *Health and Safety Laboratory Environmental Quarterly* 243.

Townsend-Small, A., S.C. Tyler, D.E. Pataki, X. Xu, and L.E. Christensen. 2012. Isotopic measurements of atmospheric methane in Los Angeles, California, USA: Influence of "Fugitive" fossil fuel emissions. *Journal of Geophysical Research: Atmospheres* 117: n/a.

Trumbore, S.E., J.B. Gaudinski, P.J. Hanson, and J.R. Southon. 2002. quantifying ecosystem-atmosphere carbon exchange with a ^{14}C Label. *EOS transactions* 83: 265–268.

Turnbull, J.C., D. Guenther, A. Karion, C. Sweeney, E. Anderson, A.E. Andrews, J. Kofler, N.L. Miles, T. Newberger, S.J. Richardson, and P.P. Tans. 2012. An integrated flask sample collection system for greenhouse gas measurements. *Atmospheric Measurement Techniques* 5: 2321–2327.

Turnbull, J.C., H. Graven, J. Miller, S. Lehmann, and Workshop Participants. 2013. Atmospheric Radiocarbon Workshop Report. *Radiocarbon* 55: 1470–1474.

Turnbull, J.C., A. Karion, M.L. Fischer, I. Faloona, T. Guilderson, S.J. Lehman, B.R. Miller, J.B. Miller, S. Montzka, T. Sherwood, S. Saripalli, C. Sweeney, and P.P. Tans. 2011. Assessment of fossil fuel carbon dioxide and other anthropogenic trace gas emissions from airborne measurements over Sacramento, California in spring 2009. *Atmospheric Chemistry and Physics* 11: 705–721.

Turnbull, J.C., E.D. Keller, W.T. Baisden, G. Brailsford, T. Bromley, M. Norris, and A. Zondervan. 2014. Atmospheric measurement of point source fossil fuel CO_2 emissions. *Atmospheric Chemistry and Physics* (in press).

Turnbull, J.C., S.J. Lehman, J.B. Miller, R.J. Sparks, J.R. Southon, and P.P. Tans. 2007. A new high precision $^{14}CO_2$ time series for North American continental air. *Journal of Geophysical Research* 112: D11310.

Turnbull, J.C., J.B. Miller, S.J. Lehman, P.P. Tans, R.J. Sparks, and J.R. Southon. 2006. Comparison of $^{14}CO_2$, CO and SF_6 as tracers for determination of recently added fossil fuel CO_2 in the atmosphere and implications for biological CO_2 exchange. *Geophysical Research Letters* 33: L01817.

Turnbull, J.C., J.B. Miller, S.J. Lehman, D.F. Hurst, W. Peters, P.P. Tans, J.R. Southon, S.A. Montzka, J.W. Elkins, D.J. Mondeel, P.A. Romashkin, N.F. Elansky, and A. Shkorokhod. 2009a. Spatial distribution of $\Delta^{14}CO_2$ across Eurasia: Measurements from the TROICA-8 expedition. *Atmospheric Chemistry and Physics* 9: 175–187.

Turnbull, J.C., P.J. Rayner, J.B. Miller, T. Naegler, P. Ciais, and A. Cozic. 2009b. On the use of $^{14}CO_2$ as a tracer for fossil fuel CO_2: Quantifying uncertainties using an atmospheric transport model. *Journal of Geophysical Research* 114: D22302.

UNSCEAR, 2000. Sources and Effects of Ionizing Radiation. UNSCEAR 2000 Report to the General Assembly, with Scientific Annexes, 1, Annex C. United Nations, New York.

Usoskin, I.G., and B. Kromer. 2005. Reconstruction of the ^{14}C production rate from measured relative abundance. *Radiocarbon* 47: 31–37.

Van Der Laan, S., U. Karstens, R.E.M. Neubert, I.T. Van Der Laan-Luijkx, and H.A.J. Meijer. 2010. Observation-based estimates of fossil fuel-derived CO_2 emissions in the Netherlands using $\Delta^{14}C$, CO and ^{222}radon. *Tellus B* 62: 389–402.

Vogel, F.R., S. Hammer, A. Steinhof, B. Kromer, and I. Levin. 2010. Implication of weekly and diurnal ^{14}C calibration on hourly estimates of CO-based fossil fuel CO_2 at a moderately polluted site in south-western Germany. *Tellus* 62: 512–520.

Vogel, J.C., A. Fuls, E. Visser, and B. Becker. 1993. Pretoria calibration curve for short-lived samples, 1930–3350 B.C. *Radiocarbon* 35: 73–85.

Weinstock, B., and H. Niki. 1972. Carbon Monoxide Balance in Nature. *Science* 176: 290–292.

Zondervan, A., and H.A.J. Meijer. 1996. Isotopic Characterisation of CO_2 sources during regional pollution events using isotopic and radiocarbon analysis. *Tellus* 48B: 601–612.